Universitetet i Stavanger

FACULTY OF SCIENCE AND TECHNOLOGY

MASTER THESIS

Study programme/specialisation: Master in Engineering Structures and Materials / Civil Engineering Structures	The spring semester, 2022 Open
Author: Danial Gorgani	
Faculty Supervisor: Professor Dimitrios Pavlou External Supervisor: Christian Linde Olsen	
Title of master's thesis: Torsional loaded towhead foundation	
Credits: 30	
Keywords: Ultimate bearing capacity Torsional loading Towhead bundle FELA FEA	Number of pages: 61 + supplemental material/other: 16 Stavanger, …15/06/2022….. date/year

Preface

This master thesis is the result of my interest in earth-related topics. The topic has been proposed by the Subsea 7 Norway Geotechnical engineering team and focuses on the ultimate capacity of shallow offshore foundations exposed to torsional loading.

The purpose of this thesis is to investigate the towhead foundation under horizontal loading that causes torsional moment by using two different approaches, namely, finite element limit analysis (FELA) and conventional finite element analysis (FEA), as well as the hand calculations according to DNV.

This report was written in the spring of 2022 for the course MKOMAS-1 21H Masteroppgave konstruksjons- og maskinteknikk at the University of Stavanger for the title of MSc degree in "Engineering Structures and Materials."

Stavanger, June 2022
Danial Gorgani

Acknowledgment

It was a pleasure to collaborate with such an experienced company, and I would like to express my sincerest gratitude to my study supervisor, Christian Linde Olsen, discipline manager of the Subsea 7 Norway geotechnical team, and Professor Dimitrios Pavlou for their invaluable guidance and knowledge.

I am also truly grateful to my colleague and dear friend, Enes Bahar for his technical support and guidance throughout my study.

Finally, I would like to appreciate the Subsea 7 geotechnical engineering team for sharing the study case and providing data for this research.

Abstract

Foundations are made to withstand and transfer loads to the soil layer beneath. Soil bearing capacity is defined as the soil's ability to support all acting loads. It is preferable to have a foundation with pure vertical loading, because the bearing capacity will be at its maximum, but this is the slightly less likely loading scenario for offshore structures. In subsea conditions, the loading is mostly coupled with vertical, horizontal, and different direction moments, which may be the effects of thermal expansion of pipelines, trawl loads, and environmental loads, thus the ultimate bearing capacity of the foundation may significantly decrease as a result of such combined loadings.

The investigated subsea structure is a towhead, which is used to connect pipeline bundles, and the foundation is rectangular with sand assumed to be beneath. Trawl load acting on the top upper corner of the towhead causes torsional loading which reduces effective bearing area, consequently lowering the ultimate capacity.

This study analyzed the ultimate bearing capacity of a towhead foundation with effects of torsional loading by using finite element limit analysis and the conventional finite element method. Hand calculations based on DNV [1] are also completed and presented in the appendix section. The finite element limit analysis approach was tested on Optum G3 software and compared to Plaxis 3D which is a strain element-based software.

Plaxis 3D software requires skilled expertise especially for the drained condition where the user must know how to assign interfaces with the accurate properties as well as make a decision on dilation angle. Furthermore, in addition to strength parameters, the deformation parameters should be assigned before initiating the analysis. However, Optum G3 runs the model with a single calculation and with only the strength parameters. The associated flow rule is taken into account in the limit analysis, so the user is not required to decide on a dilatancy angle. Collapse load is between upper and lower bound solutions, providing users with an accuracy mechanism to check the result. Furthermore, the Optum G3 analysis duration was significantly shorter than that of Plaxis 3D with the long run times of each case.

Although the minimum deadweight calculated with the 3D finite element approach with Optum G3 and Plaxis 3D are similar, the most challenging aspect of working with Plaxis 3D was the lack of an accuracy mechanism to check on the final result, the only solution for it may be to compute several stress-strain curves with more elements and finer meshes, which is very time

- consuming process. Additionally, VH diagrams constructed for comparison of Optum G3 and hand calculation results define a perfect fit of FELA.

TABLE OF CONTENTS

Preface ..... **I**

Acknowledgment ..... **III**

Abstract ..... **V**

TABLE OF CONTENTS ..... **VII**

List of figures ..... **X**

List of tables ..... **XII**

Notation ..... **XIII**

Chaper 1: Introduction **1**

1.1 Background of thesis *1*

1.2 Motivation of thesis *4*

1.3 Objectives *5*

1.4 Limitations *5*

1.5 Structure of the Thesis *5*

Chaper 2: Theoretical background **6**

2.1 Introduction *6*

2.2 Bearing capacity *6*

2.2.1 Terzaghi's theory 8

2.2.2 Meyerhof's theory 10

2.2.3 Brinch Hansen Method 12

2.2.4 Suggested solution by Vesic 14

2.2.5 Michalowski's Approach 14

2.3 Combined loading of shallow foundations *15*

2.3.1 Stability envelope 16

2.3.2 Effective area calculation 16

Chaper 3: Numerical analysis **20**

3.1 Introduction *20*

3.2 Limit Analysis *20*
3.2.1 Lower Bound Theorem 20
3.2.2 Upper Bound Theorem 21
3.3 Finite Element Limit Analysis *21*
3.4 Utilized software for FELA *22*
3.4.1 Limit analysis approach in Optum G3 23
3.4.2 Governing equations 24
3.4.3 Lower bound FELA 26
3.4.4 Upper bound FELA 27
3.4.5 Elastoplastic analysis in Optum G3 27
3.4.6 Adaptive mesh 27
3.4.7 Flow rule effects 28
3.5 Finite element analysis *30*
3.6 Utilized software for FEA *30*
3.6.1 Mesh generation 33
Chaper 4: Results of numerical analysis **33**
4.1 Optum G3 ..... *33*
4.1.1 The geometry of the model 33
4.1.2 Soil properties and interfaces 34
4.1.3 Mesh generation 35
4.1.4 Results 36
4.2 Plaxis 3D *37*
4.2.1 The geometry of the study 37
4.2.2 Input materials 38
4.2.3 Mesh Generation of the model 39
4.2.4 Point selection for curve generation 41
4.2.5 Results 41
Chaper 5: Discussion of the results **47**
Chaper 6: Conclusion and recommendation for future works **50**
6.1 Conclusion *50*
6.2 Recommendation for future works *50*
Chaper 7: References **51**

Chaper 8: Appendices..... 53

8.1 Hand calculations 53

8.1.1 The effective area of foundation 53

8.1.2 Towhead foundation stability envelope 58

List of figures

Figure 1-1 Typical towhead structure [3] 2

Figure 1-2: Pipeline bundle [2] 2

Figure 1-3: Typical bundle drag arrangement [4] 3

Figure 1-4: Bottom trawl [5] 4

Figure 2-1: Different types of failure modes [6] 7

Figure 2-2: Failure edges of strip footing [7] 8

Figure 2-3: Derivation of bearing capacity equation [7] 9

Figure 2-4: Calculation of Nγ based on Lundgren-Mortensen mechanism of failure [10] 12

Figure 2-5: General case of retaining wall with ground and base inclination [10] 14

Figure 2-6: Effect of dilatancy angle on Nγ (redrawn after [12]) 15

Figure 2-7: Combined vertical and horizontal foundation stability envelope [1] 16

Figure 2-8: Eccentric loading of foundation and equivalent stress distribution. [15] 17

Figure 2-9: Effective area of bearing, redrawn from [15] 18

Figure 2-10: Determination of load T, redrawn from [16] 19

Figure 3-1: 2D Sign convention [21] 23

Figure 3-2: Interval of upper and lower bound solutions for different meshes 23

Figure 3-3: Solid with volume V and boundary of S subjected to tractions [19] 24

Figure 3-4: Load displacement curve for associated and nonassociated flow rule [19] 28

Figure 3-5: Rigid block on the frictional surface [19] 29

Figure 3-6: Sign convention [27] 32

Figure 3-7: 10-node tetrahedron element [27] 32

Figure 3-8: Boundary conditions 33

Figure 4-1: Geometry and soil domain 34

Figure 4-2: Mesh generation with 10.000 elements 35

Figure 4-3: Convergence of load with different element sizes 36

Figure 4-4: Failure mechanism of towhead 37

Figure 4-5: Plaxis 3D model of towhead on soil domain 38

Figure 4-6: Plaxis 3D Different mesh generation with predefined patterns 40

Figure 4-7: Mesh generation and refinement around the foundation 40

Figure 4-8: Selected point for curve generation 41
Figure 4-9: Load-displacement curve for all cases 42
Figure 4-10: Deformed mesh with 2350 kN vertical load and trawl load 43
Figure 4-11: Shear stress distribution 44
Figure 4-12: Incremental displacement 45
Figure 4-13: Cross-sections of incremental displacement 46
Figure 5-1: Summary of the results 47
Figure 5-2: Comparison of HV diagrams [28] 49
Figure 5-3: Foundation stability envelope derived by Optum G3 and hand calculations according to DNV 49
Figure 8-1: Towhead model dimension and trawl loading 53
Figure 8-2: Foundation stability envelope 61

List of tables

Table 4-1: Soil domain and towhead dimensions – Optum G3 34

Table 4-2: Input soil properties 35

Table 4-3: Soil domain and towhead dimensions – Plaxis 3D 37

Table 4-4: Soil model properties 38

Table 4-5: Plate properties 39

Table 4-6: Number of elements and nodes for different element distribution 39

Table 4-7: Load cases 42

Table 4-8: Loading coordinates 42

Table 8-1: 2000 kN weight sliding check 55

Table 8-2: 2540 kN. weight sliding check 57

Table 8-3: Input data 59

Table 8-4: Bearing capacity calculation 59

Notation

List of symbols

Symbol	Definition	Unit
A	Foundation area	[m^2]
A_{eff}	Effective foundation area	[m2]
B	Foundation width	[m]
B_{eff}	Effective foundation width	[m]
c	Soil cohesion	[kN/m^2]
d_c, d_q, d_γ	Depth factors of bearing capacity equation	[-]
e	Eccentricity	[m]
E'_{ref}	Young's modulus	kPa
e_x,e_z	Eccentricity in x and z axis	[m]
F_x,F_y,F_z	Loads in x,y and z axis	[kN]
H	Horizontal force	[kN]
H'	Equivalent horizontal force	[kN]
i_c, i_q, i_γ	Inclination factors of bearing capacity equation	[-]
L	Foundation length	[m]
L_{eff}	Effective foundation length	[m]
M_x,M_y,M_z	Moments in x,y and z axis	[kN.m]
N_c, N_q, N_γ	Bearing capacity factors	[-]
P_p	Reaction force	[kN]
q_u	Ultimate bearing capacity	[kN/m^2]
R_x, R_y	Reaction forces in x and y axis	[kN]
s_c, s_q, s_γ	Shape factors of bearing capacity equation	[-]
V	Vertical force	[kN]
β	The slope angle	[˚]
γ	Unit weight	[kN/m^3]
γ'	Effective unit weight	[kN/m^3]
τ	Shear stress	[N/mm^2]
φ	Friction angle	[˚]
ψ	Dilatancy angle	[˚]

List of abbreviations

2D	Two-dimensional
3D	Three-dimensional
DNV	Det norske veritas
FEA	Finite element analysis
FELA	Finite element limit analysis
FEM	Finite element method
FoS	Factor of safety
GC	Geometrical center
HS	Hardening soil
LB	Lower bound
MC	Mohr-coloumb
SLS	Serviceability limit state.
UB	Upper bound
ULS	Ultimate limit state
V/H	Vertical/ Horizontal

Chaper 1: Introduction

1.1 Background of thesis

Offshore geotechnical engineering deals with the geotechnical-related design, construction, and demobilization of structures in the subsea environment. Shallow foundations, gravity-based, monopiles, jacket-piles, and suction caissons are some of the foundation types used for offshore structures. Shallow foundations are characterized as embedment depths that are generally equal to or less than four times the width of the foundation.
This report will investigate a shallow towhead foundation resting on the sand. According to [1] Most foundation stability analyses are carried out using the conventional limit equilibrium method, which is satisfied by verifying the equilibrium between design loads and capacities. Although the conventional bearing capacity approach is adequate for the preliminary stages of design for gravity-based offshore structures, it is insufficient for detailed calculations for foundation stability, because in this approach, several failure surfaces must be accessed to find the critical one, however, this problem can be solved by using the finite element method, which allows visualizing the failure surface in each part of the analysis.

Shallow foundations are being installed for many infrastructures in the offshore industry. A towhead is a type of structure that allows pipeline bundles such as valve work, pipelines, and control systems to be connected to a single structure. Towhead manifolds control the well, flow, and production flow rates. Towheads do have the benefit of being a cost-effective solution by reducing installation time which avoids trenching and burying activities. [2] (See Figure 1-1 and Figure 1-2)

Figure 1-1 Typical towhead structure [3]

Figure 1-2: Pipeline bundle [2]

Towheads are built on-site and utilized to drag the pipeline bundle to the field by two vessels, one leading, one trailing, and one patrol or survey vessel assisting. as illustrated in Figure 1-3. During the drag, buoyancy tanks will be attached to towheads to make them buoyant until reaching the target area which is known as the controlled depth tow method. [4]

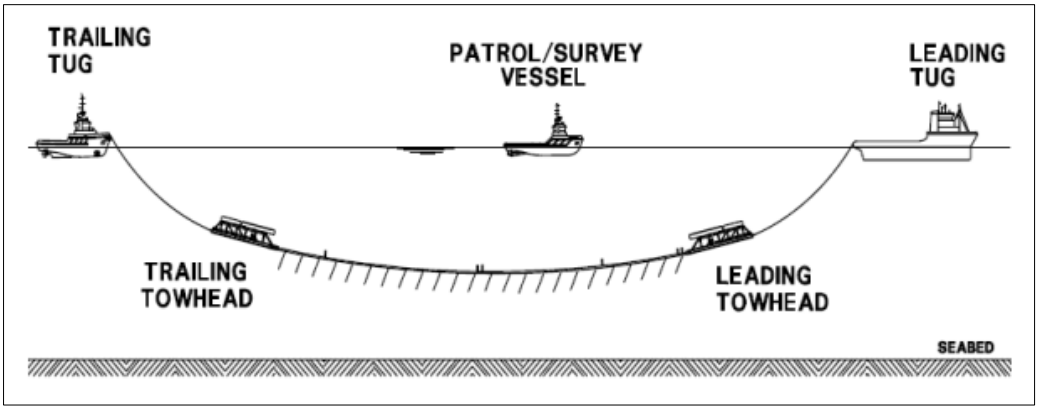

Figure 1-3: Typical bundle drag arrangement [4]

This report will investigate the effect of trawl load on towhead foundation, which causes torsional moment, this type of load is governing design load for towhead structures. The main intention of this thesis is to find the towhead with the smallest possible weight, hence the reduced towhead weight may save structural steel and reduces base handling difficulties along with transportation costs resulting in the use of a smaller installation vessel.

Unprotected towhead bundle may exposed to trawl load. Bottom trawls are cone-shaped nets pulled by vessels along the seafloor. As illustrated in Figure 1-4, warp lines connect the trawl doors to the vessel and sweep lines connect it to the trawl net. Trawl floats, ground gear, and trawl doors keep the net open. The trawl doors used by present vessels can weigh up to 5-6 tonnes. According to [5] a trawler vessel traveling at 4 knots with a 200-meter-wide trawl net will expose 1,500,000 m2 of seabed area for every hour of trawling activity.

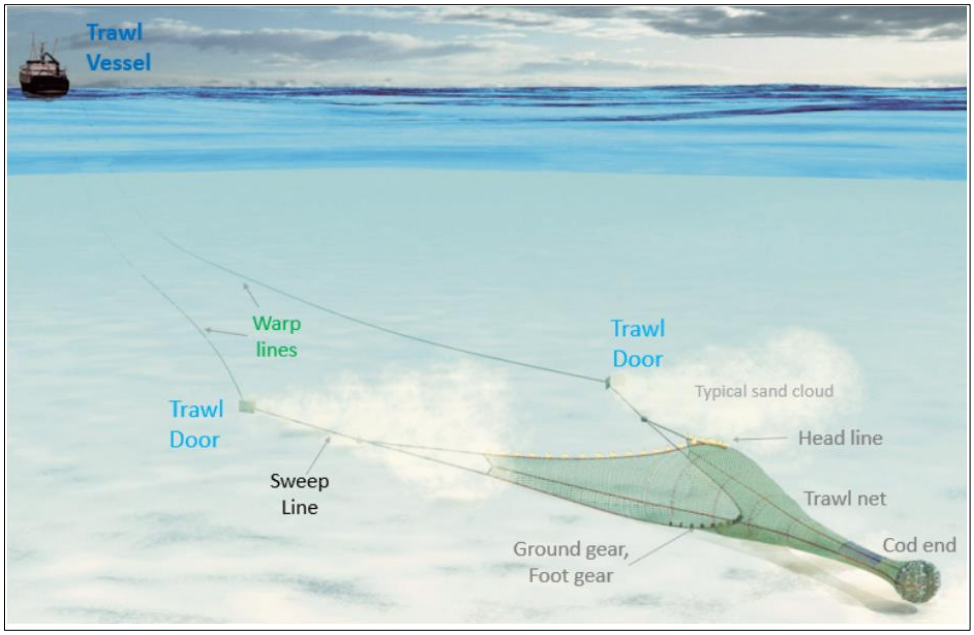

Figure 1-4: Bottom trawl [5]

1.2 Motivation of thesis

Torsion moments can occur when horizontal loads are applied off-center of a foundation, when these loads act with an eccentricity will lead to generation of additional forces and moments on the foundation, resulting in a reduction of effective bearing area and an uneven distribution of shear stress. When the above situations of eccentric combined loading occur, there will be a significant reduction in ultimate bearing capacity which is a highly 3D-dependent problem. Furthermore, this type of loading has the potential to cause the subsea structure to slide, overturn or fail as a bearing failure.

When different methods are used, different outcomes may be expected. However, this thesis will discuss the outstanding features of the FELA method over the traditional FEA approach with an evaluation of the minimum safe weight for torsional loaded towhead foundation resting on the sand by using two different finite element-based programs, Optum G3 and Plaxis 3D, as well as hand calculations with a comparison of all results.

1.3 Objectives

The primary objectives of this thesis are listed as follows,

1. Overview of current methods for calculation of ultimate bearing capacity for the shallow foundation.
2. Numerical analysis of the case and checking the validity of conventional methods.
3. Evaluation of fixed overturning and torsional moments from trawl load that affects bearing capacity and calculating the minimum weight of the towhead on the sand with Optum G3 and Plaxis 3D.
4. Summary and discussion of all results.

1.4 Limitations

In all calculation steps in this thesis,

- Only one fixed geometry is considered to be the same as a typical towhead bundle.
- The material and load factor are assumed to be 1.00.
- Only one fixed static load case with overturning and torsional moment components from the horizontal load is considered.
- Seismic loads are not taken into account.
- For the entire analysis, only one soil model was employed, and it was sand with Mohr-Coulomb failure criteria.

1.5 Structure of the Thesis

Chapter 1 – Introduction
The general background and motivation for work are presented in this chapter.

Chapter 2 – Theoretical background
This chapter will present conventional methods for calculating the ultimate bearing capacity for shallow foundations.

Chapter 3 – Numerical analysis
This chapter will provide a theoretical background of limit analysis and limit equilibrium. Also, summaries of programs used for each method will be presented.

Chapter 4 – Results of numerical analysis
Within this chapter, the results of all approaches will be given in detail.

Chapter 5 – Discussion of the results
Here, there will be a discussion and comparison of the results, as well as recommendations for further studies.

Chapter 6 – Conclusion and recommendation for future works
This section will contain the study's conclusion and recommendations for future research.

Chaper 2: Theoretical background

2.1 Introduction

This section is based on published geotechnical engineering books, articles, and design codes. It provides background information on the general bearing capacity equation of various approaches, as well as the DNV recommendation for design methods, which includes the stability envelope concept with effective bearing area consideration.

2.2 Bearing capacity

Bearing capacity is the adequacy of foundations to carry all the upcoming loads and direct them to the soil underlying, ultimate bearing capacity is the maximum applied contact pressure between the base of the foundation and the soil beneath at which the shear failure mechanism starts to develop.
There are three main shapes of failure in soil mechanics, according to [6] the shear failure modes of foundation can be described as follows,

- General shear failure
- Local shear failure
- Punching shear failure

General shear failure is a continuous failure line that occurs between the side of the footing and the soil beneath. The load increases to a maximum which is denoted as q_u "The ultimate load". (See Figure 2-1a)

In local shear failure, the failure surface is not continuous like the general failure and some heaving at ground level may be observed. (See Figure 2-1b) and the punching failure will cause compression of underlying soil mass and it will act almost vertical as can be seen from Figure 2-1c.

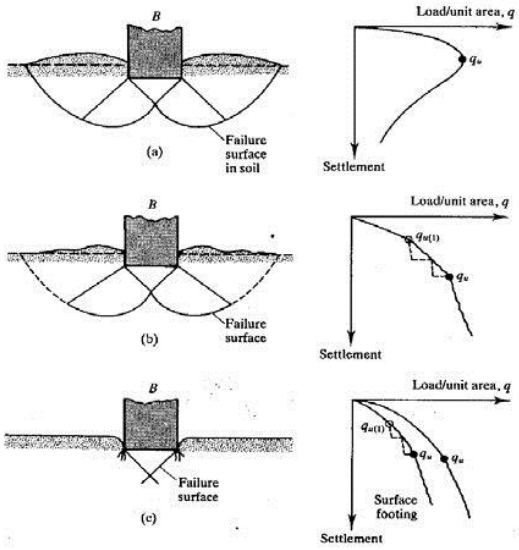

Figure 2-1: Different types of failure modes [6]

From the Figure 2-1 it can be seen that the general behavior of load-settlement curves is identical to each other, in general, shear failure mode when the curves reach a steady maximum value is denoted as failure point, however, for local and punching shear failure modes the failure point defines the point where it corresponds to unacceptable deformation.

Geotechnical engineering has faced challenges in determining the exact solution to the bearing capacity equation for drained conditions. There are several approaches to calculating bearing capacity and related coefficients, but this thesis will go over the three most referenced solutions of Terzaghi and Meyerhof bearing capacity theories with the enhanced method by Brinch Hansen.

Also, Michalowski and Vesic approaches for bearing capacity coefficient N_γ will be presented at the end of this section.

2.2.1 Terzaghi's theory

Terzaghi was one of the pioneers to present an extensive theory for the assessment of ultimate bearing capacity, which has been used extensively in geotechnical engineering practices. Proposed failure edges of the strip foundation can be seen in Figure 2-2. [7]

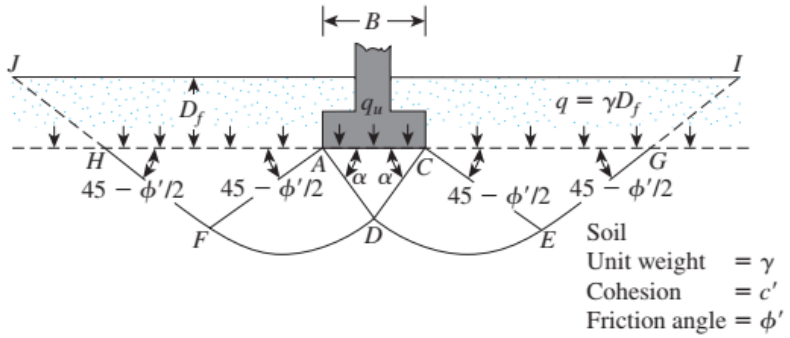

Figure 2-2: Failure edges of strip footing [7]

There are three different zones namely, the triangular zone ADC, radial shear zone CDE and ADF, and Rankie passive zones CEG and AFH. The inclination of line AD and CD are denoted as internal friction angle φ. The ultimate bearing capacity of a shallow foundation is developed by equilibrium in triangle ACD. With applied q_u there will be a reaction force of P_p acting in the opposite direction as shown in Figure 2-3, the inclination of P_p load is equal to friction angel φ so the equation (2.1) is derived by equilibrium in triangle ACD.

$$q_u \cdot 2b \cdot 1 = 2C \cdot Sin\varphi' + 2P_p - W \tag{2.1}$$

Where,

b = B/2

C is the cohesive force acting on lines DA and DC which corresponds to $C = c' \cdot b/\cos(\varphi')$

W is the weight of the soil mass in triangle ACD, $W = \gamma b^2 \tan\varphi'$

Equation (2.1) can be rewritten as follow,

$$q_u = \frac{P_p}{b} + c'tan\varphi - \frac{\gamma b}{2}\tan\varphi \tag{2.2}$$

It can be seen from equation (2.2) that the passive pressure P_p is the summation of influences from soil weight, cohesion, and surcharge.

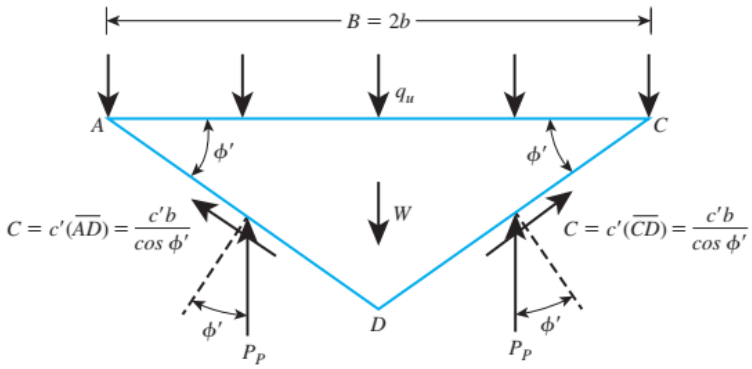

Figure 2-3: Derivation of bearing capacity equation [7]

The final solution of Terzaghi's approach is shown in equation (2.3)

$$\mathrm{q_u = c'N_c + qN_q + \frac{1}{2}\gamma BN_\gamma} \tag{2.3}$$

$$\mathrm{N_c = tan\varphi(K_c + 1)} \tag{2.4}$$

$$\mathrm{N_q = K_q tan\varphi'} \tag{2.5}$$

$$\mathrm{N_\gamma = \frac{1}{2}tan\varphi(K_\gamma tan\varphi - 1)} \tag{2.6}$$

$\mathrm{N_c}$, $\mathrm{N_q}$ and $\mathrm{N_\gamma}$ are bearing capacity factors that contribute to cohesion, surcharge, and soil weight respectively. Terzaghi used the approximation method to evaluate the values for $\mathrm{K_c}$, $\mathrm{K_q}$ and $\mathrm{K_\gamma}$.

It is followed by an estimation of ultimate bearing capacity for square and circular foundations, as can be seen from equation (2.7) -square footing- and equation (2.8) -circular footing- where B is the foundation width, for circular footing it is the diameter of the foundation. For both foundations, the contribution of cohesion has increased by 30% and the contribution of soil weight decreased by 20% for square footing and in the same way 40% for circular footing. [7]

$$q_u = 1.3c'N_c + qN_q + 0.4\gamma BN_\gamma \quad (2.7)$$

$$q_u = 1.3c'N_c + qN_q + 0.3\gamma BN_\gamma \quad (2.8)$$

2.2.2 Meyerhof's theory

Meyerhof's bearing capacity method is an extension of one developed by Terzaghi. He did not take into account the overburden soil contribution to shear resistance, which Meyerhof did, and he introduced depth and shape factors that have a desirable effect on the ultimate bearing capacity of a foundation in different shape and depth conditions. [8]

Equations (2.9) show the general bearing capacity formula for inclined loading derived by Meyerhof [7],

$$q_u = s_c d_c i_c c N_c + s_q d_q i_q q N_q + s_\gamma d_\gamma i_\gamma 0.5\gamma B N_\gamma \quad (2.9)$$

N_c, N_q and N_γ are factors of bearing capacity for a strip footing, s_c, s_q and s_γ are shape factors and depth of the footing considered by introducing new factors as d_c, d_q and d_γ, for the inclination of loading case factors are i_c, i_q and i_γ.

Equations for derived bearing capacity factors are as follows,

Shape factors,

$$s_c = 1 + 0.2\frac{B}{L}tan^2\left(45 + \frac{\varphi}{2}\right) \quad (2.10)$$

$$s_q = s_\gamma = 1 + 0.1\frac{B}{L}tan^2\left(45 + \frac{\varphi}{2}\right) \quad \text{for } \varphi \geq 10^\circ \quad (2.11)$$

$$s_\gamma = s_q = 1 \quad \text{for } \varphi = 0 \quad (2.12)$$

Depth factors,

$$d_c = 1 + 0.2\,\frac{D_f}{B}\tan\left(45 + \frac{\varphi}{2}\right) \tag{2.13}$$

$$d_q = d_\gamma = 1 + 0.1\frac{D_f}{B}\tan\left(45 + \frac{\varphi}{2}\right) \quad \text{for } \varphi \geq 10^\circ \tag{2.14}$$

$$d_q = d_\gamma = 1 \quad \text{for } \varphi = 0 \tag{2.15}$$

Inclination factors,

$$i_c = i_q = \left(1 - \frac{\alpha^\circ}{90^\circ}\right)^2 \tag{2.16}$$

$$i_\gamma = \left(1 - \frac{\alpha^\circ}{\varphi}\right)^2 \quad \text{for } \varphi \geq 10^\circ \tag{2.17}$$

$$i_\gamma = 1 \quad \text{for } \varphi = 0 \tag{2.18}$$

It should be noted that α in equations (2.16) and (2.17) is the inclination of the footing load and the unit is degree.

Bearing capacity factors N_c and N_q is the same as the suggested one by Reissner (1924) and Prandtl (1921). [9]

$$N_q = e^{(\pi \cdot \tan\varphi)}\tan^2\left(45 + \frac{\varphi}{2}\right) \tag{2.19}$$

$$N_c = (N_q - 1)\cot\varphi \tag{2.20}$$

Meyerhof identified N_γ factor,

$$N_\gamma = (N_q - 1)\tan(1.4\varphi) \tag{2.21}$$

It should also be mentioned that bearing capacity coefficients are all dependent on friction angle (φ).

2.2.3 Brinch Hansen Method

Hansen's general bearing capacity formula was a modification of Meyerhof's by including two new factors as base and ground inclination factors denoted as b and g.

$$q_u = \frac{1}{2}\gamma B N_\gamma s_\gamma d_\gamma i_\gamma b_\gamma g_\gamma + q N_q s_q d_q i_q b_q g_q + c N_c s_c d_c i_c b_c g_c \quad (2.22)$$

According to [10], the bearing capacity factor N_γ calculated by Lundgren-Mortensen was the best approach, while the N_c and N_q factors are the same as Reissner (1924) and Prandtl (1921) approaches. [10]

$$N_\gamma = 1.5(N_q - 1)\tan(\varphi) \quad (2.23)$$

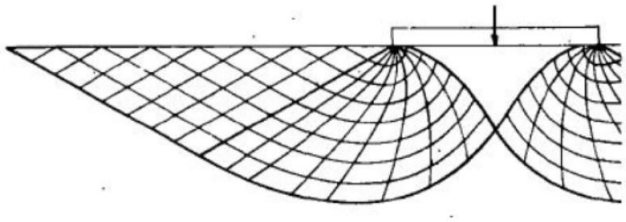

Figure 2-4: Calculation of N_γ based on Lundgren-Mortensen mechanism of failure [10]

Hansen's proposed bearing capacity factors are as follows,

Shape factors,

$$s_q = 1 + \left(\frac{B}{L}\right)\sin(\varphi) \quad (2.24)$$

$$s_\gamma = 1 - 0.4\left(\frac{B}{L}\right) \quad (2.25)$$

Load inclination factors should not be used if the value becomes negative,

$$i_q = \left(1 - \frac{0.5 \cdot H}{V + A \cdot c \cdot \cot\varphi}\right)^5 \quad (2.26)$$

$$i_\gamma = \left(1 - \frac{0.7 \cdot H}{V + A \cdot c \cdot \cot\varphi}\right)^5 \tag{2.27}$$

The depth factor suggested by Hansen is valid for both shallow and deep foundations,

$$\begin{aligned} d_q &= 1 + 2\tan\varphi \cdot (1 - \sin\varphi)^2 \cdot \frac{D}{B} \\ d_c &= 0.4\frac{D}{B} \qquad \text{for } \frac{D}{B} < 1 \\ d_\gamma &= 1.00 \end{aligned} \tag{2.28}$$

$$\begin{aligned} d_q &= 1 + 2\tan\varphi \cdot (1 - \sin\varphi)^2 \cdot arc\ tan\frac{D}{B} \\ d_c &= 0.4 \cdot arc\ tan\frac{D}{B} \qquad \text{for } \frac{D}{B} > 1 \\ d_\gamma &= 1.00 \end{aligned} \tag{2.29}$$

Inclination factors for ground and foundation base,

For the case of frictionless soil ($\varphi = 0$) the exact formula for base and ground inclination is as follows,

$$b_c = \frac{\eta^\circ}{147^\circ} \tag{2.30}$$

$$g_c = \frac{\beta^\circ}{147^\circ} \tag{2.31}$$

Where β and η are ground and footing inclinations in degree.

For the cases with $\varphi > 0$ following factors can be used,

$$b_q = e^{-2\eta tan\varphi} \tag{2.32}$$

$$b_\gamma = e^{-2.7\eta tan\varphi} \tag{2.33}$$

$$g_q = g_\gamma = [1 - 0.5 \cdot tan\beta]^5 \tag{2.34}$$

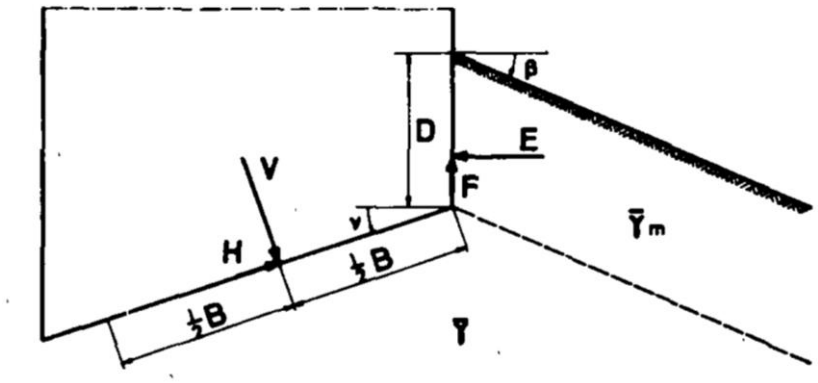

Figure 2-5: General case of retaining wall with ground and base inclination [10]

2.2.4 Suggested solution by Vesic

The Vesic procedure is mainly same as Hansen's method; the N_c and N_q factors are same, however, he proposed a new N_γ that differs slightly from Hansen's approach [11],

$$N_\gamma = 2(N_q + 1)\tan(\varphi) \tag{2.35}$$

2.2.5 Michalowski's Approach

Michalowski [12] used the kinematical approach of limit analysis by assuming perfectly plastic material behavior to evaluate the influence of soil weight coefficient (N_γ) on ultimate bearing capacity. According to Michalowski, the bearing capacity factor N_γ becomes more conservative with increasing soil cohesion and foundation depth, also he found that dilatancy angle (ψ) affects on N_γ coefficient.

$$N_\gamma = e^{0.66+5.11\cdot tan\varphi^*}\, tan\varphi^* \tag{2.36}$$

$$N_\gamma = e^{5.11\cdot tan\varphi^*}\, tan\varphi^* \tag{2.37}$$

$$tan\varphi^* = \frac{cos\psi \cdot \sin\varphi}{1 - sin\psi \cdot \sin\varphi} \tag{2.38}$$

Equation (2.36) is valid for rough footings and (2.37) for smooth footings. According to [12] flow rule has a negligible effect on N_γ for friction angles less than 25°, however, for friction angles greater than 25° this effect has considerable contribution as it is shown in Figure 2-6.

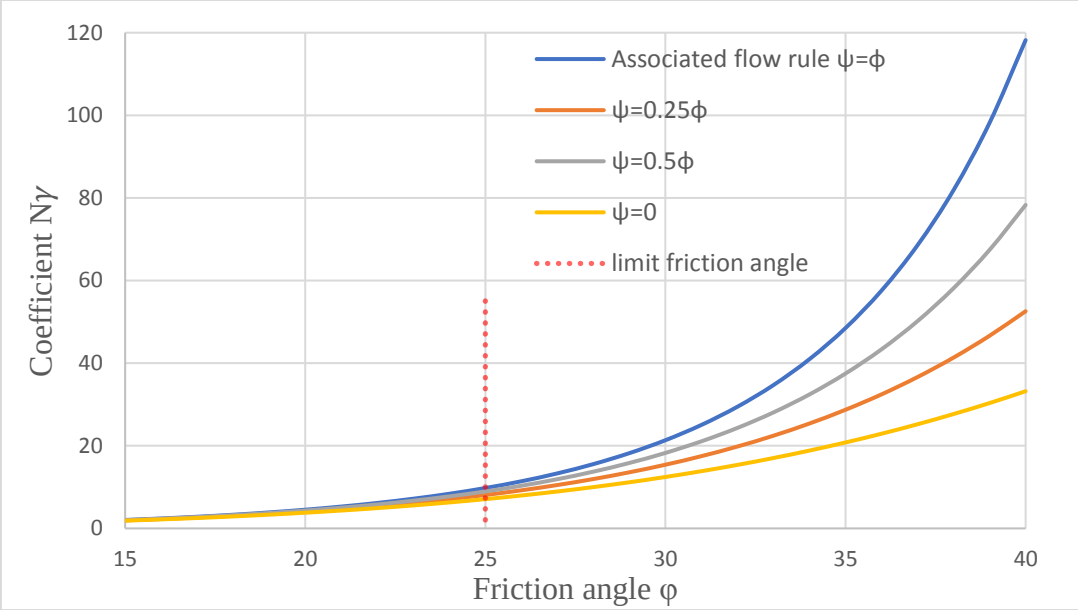

Figure 2-6: Effect of dilatancy angle on N_γ (redrawn after [12])

2.3 Combined loading of shallow foundations

It has been always desirable to design a shallow foundation in a way that resultant forces act on the centroid of the foundation however, this is not the case in geotechnical engineering practices. Especially when it comes to subsea shallow foundations, these types of foundations are subjected to different types of loading, these eccentric loading may cause by thermal loads of pipeline or trawl loads acting with inclination. [13]

As previously discussed, in presence of inclined loading of the foundation the inclination coefficients have been suggested in addition to the other factors of the general bearing capacity equation. However, bearing capacity cannot be predicted accurately for complex load configurations, because of the experimental nature of the bearing capacity coefficients, thus, this approach was modified to the construction of a failure envelope to define the ultimate bearing capacity related to the maximum vertical and horizontal loads which cause the failure of the foundation. [14]

2.3.1 Stability envelope

The stability envelope approach is used to estimate the ultimate bearing capacity of a shallow foundation subjected to both inclined and eccentric loads. This approach defines a region along which all allowable load combinations must lie. Also, it is crucial to check the sliding capacity as well as the bearing capacity of gravity-based offshore foundations since failure may involve horizontal sliding. Figure 2-7 shows different stability envelopes for drained conditions. The results are presented as a foundation stability envelope for horizontal and vertical load combinations with a horizontal sliding capacity curve cut-off. Bearing capacity curves are defined for both eccentric and non-eccentric loadings, the eccentricity also designates consideration of the effective area that will be used in further calculations. [1]

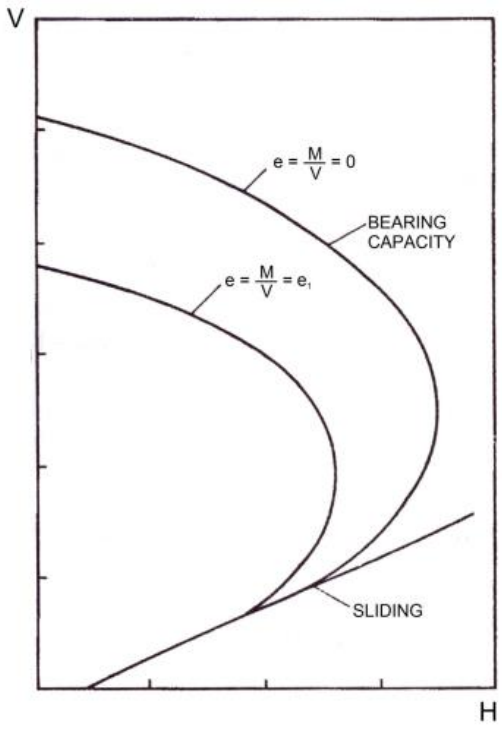

Figure 2-7: Combined vertical and horizontal foundation stability envelope [1]

2.3.2 Effective area calculation

With the presence of eccentric loads, the shallow foundation will be subjected to moment and torsion, as a consequence the ultimate bearing capacity of the foundation will reduce

significantly because the bearing area of the foundation will decrease, according to [10] all acting vertical and horizontal forces converted to one resultant component and reduction on bearing area or "effective area" is specified in the manner that resultant loads overlap the geometrical center.

The eccentricity changes the bearing pressure underneath the foundation to a nonlinear form, the equivalent loading with eccentricity is shown in Figure 2-8 where the load P is acting with a moment leg of e_B from geometrical centroid of foundation, the eccentricity in the width direction e_B defined as, [15]

$$e_{\mathrm{B}} = \frac{\mathrm{M_B}}{\mathrm{P}} \tag{2.39}$$

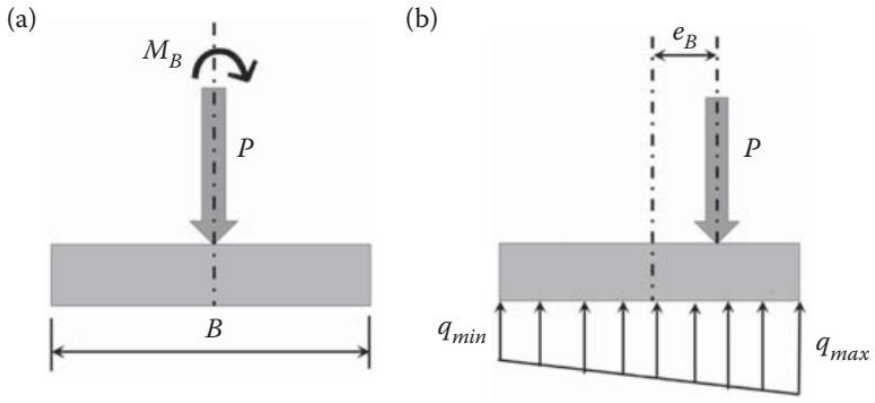

Figure 2-8: Eccentric loading of foundation and equivalent stress distribution. [15]

The eccentricity in the Length direction is shown on (2.40), $\mathrm{M_L}$ is the applied moment which is perpendicular to the width (B) axis,

$$e_{\mathrm{L}} = \frac{\mathrm{M_L}}{\mathrm{P}} \tag{2.40}$$

Effective length and width are as follows,

$$B_{eff} = B - 2 \cdot |e_B| \tag{2.41}$$

$$L_{eff} = B - 2 \cdot |e_L| \tag{2.42}$$

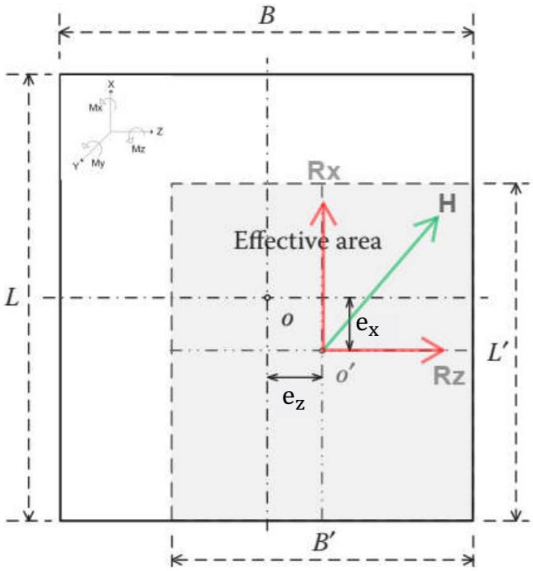

Figure 2-9: Effective area of bearing, redrawn from [15]

As shown in Figure 2-9, after assigning the sign convention for effective area calculation, the eccentricity notations have changed accordingly.

$$e_z = \frac{M_x}{P} \tag{2.43}$$

$$e_x = \frac{M_z}{P} \tag{2.44}$$

$$B_{eff} = B - 2 \cdot |e_z| \tag{2.45}$$

$$L_{eff} = B - 2 \cdot |e_x| \tag{2.46}$$

Shear stress is assumed to be distributed evenly on the effective area, thus the forces R_x and R_z are converted to equivalent force H,

$$H = \sqrt{\left({R_x}^2 + {R_z}^2\right)} \tag{2.47}$$

By general disposition, forces are distributed over the effective area (Figure 2-10c.), and force T could be defined by moment equilibrium about the center (Figure 2-10d.).

$$\begin{gathered} M_y - \mathrm{T} \cdot \left(\frac{L_{eff} - x}{2} + \frac{x}{2}\right) = 0 \\ T = \frac{2 \cdot M_y}{L_{eff}} \end{gathered} \tag{2.48}$$

According to [1] in presence of torsional moment to the foundation in addition to horizontal and vertical loads, the interaction of these forces should be taken into account in the ultimate bearing capacity calculation, equivalent horizontal force H' is given as,

$$\begin{gathered} H' = \tau \cdot \mathrm{A}_{eff} = \mathrm{T} + \sqrt{H^2 + T^2} \\ H' = \frac{2 \cdot \mathrm{M_y}}{\mathrm{l_{eff}}} + \sqrt{\left(\sqrt{\left({R_x}^2 + {R_z}^2\right)}\right)^2 + \left(\frac{2 \cdot \mathrm{M_y}}{\mathrm{l_{eff}}}\right)^2} \end{gathered} \tag{2.49}$$

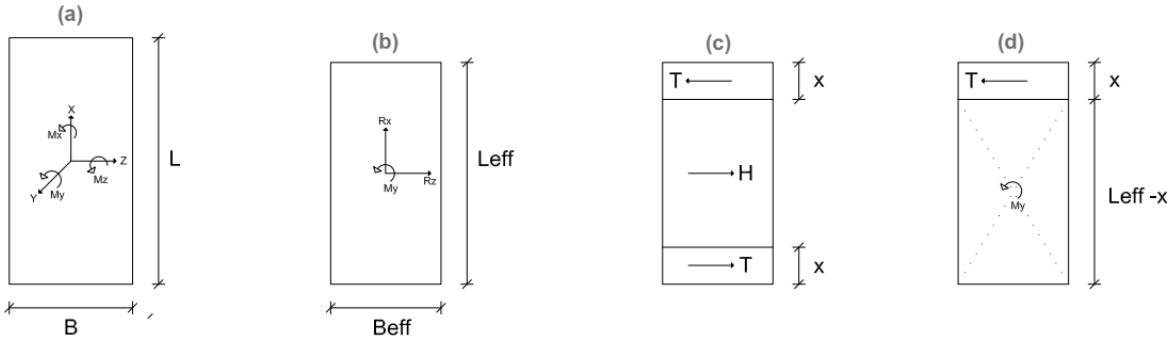

Figure 2-10: Determination of load T, redrawn from [16]

The requirement for the sliding capacity of the foundation is shown in equation (2.50) where P is the vertical load and φ is reduced sliding friction angle.

$$H' \leq \mathrm{P} \cdot \tan \varphi \tag{2.50}$$

Chaper 3: Numerical analysis

3.1 Introduction

This section presents the theory behind methods for ultimate capacity analysis of the foundations, it will follow by giving more details on the finite element approach of software that is implemented on those approaches. To compare the ultimate capacity of towhead bundle, two different finite element based software were used, first one is Optum G3 which is a finite element limit analysis based software, and the other one is Plaxis 3D which is based on strain type element, further details of Optum G3 and Plaxis 3D are also presented in this section.

3.2 Limit Analysis

Limit analysis was firstly developed by Drucker et al. (1951) and it corresponds to utilize of upper bound and lower bound of plasticity theorems. [17] The plasticity theorem allows for the upper and lower bounds to be obtained in a single-step calculation, enables the estimation of the collapse load without iterating the full displacement curve, and it is based on the plastic boundary theorem with assumptions of small deformations for a perfectly plastic material with associated flow rule and the plastic strain rates are normal to the yield surface. When a perfectly plastic soil is mass-loaded, it will first reach the elastic region and with the increasing load, it will become partially plastic, the last phase is when the load reaches the critical value which is called collapse load, hence the plastic collapse occurs when deformation increases with the same loading.

The primary objective of limit analysis is to compute the lower and upper bounds of true collapse load for a soil mass with given strength parameters and boundary conditions.

3.2.1 Lower Bound Theorem

The lower bound theorem is based on a statically admissible stress field, in any stress field of perfectly plastic material, the applied loads would not cause any failure when the conditions are

satisfied. A statically admissible solution requires equilibrium of applied loads and internal stresses so they overcome load by stress filed which is statically admissible is lower bound of the true limit load. [18]. It is the static part of governing equilibrium equations and yield criteria.

According to [15], if all geometric changes during collapse are ignored, a statically admissible collapse load F_c^s is always less than or equal to the exact collapse load F_c ($F_c^s \leq F_c$). The load derived from a statically admissible stress field F_c^s is a lower bound on the true collapse load, F_c.

3.2.2 Upper Bound Theorem

In opposition to the lower bound theorem, the upper bound theorem is based on the kinematically admissible solution which fulfills the plastic flow rule and velocity boundary conditions and is derived from the equilibrium between dissipated work by external and internal loads caused by plastic deformation. [18] In other words, the structure will collapse when the external work done is equal to the internal.

According to [15], if all geometric changes during collapse are ignored, a kinematically admissible collapse load F_c^k is always greater or equal to the exact collapse load F_c ($F_c^k \geq F_c$). The load derived from a kinematically admissible stress field F_c^k is an upper bound on the true collapse load, F_c.

3.3 Finite Element Limit Analysis

Finite element limit analysis is a recently developed method that makes it possible to discrete the soil domain to finite elements and with the use of upper and lower bounds of plasticity theory determines the collapse load bounds in contrast to conventional finite element method, thus the exact solution is between upper and lowers bound. [15]
FELA incorporates classical plasticity theorem with finite elements to provide robust upper and lower bounds of collapse or failure load. This approach is slightly different than conventional finite element analysis, even though both methods are based on the concept of discretization. [18]

3.4 Utilized software for FELA

For the evaluation of the ultimate capacity of the foundation with limit analysis, Optum G3 is used. It is the first commercially available 3D finite element limit analysis software, and it offers various types of analysis for complex stability problems in geotechnical engineering. Since the user interface is comparable to any other 3D modeling tool, with no hidden buttons or commands, the user can easily model and analyze the geotechnical problem. This section will go through the fundamentals of Optum G3 and a brief introduction to the theory of the software will be given from [19].

A summary of the most important features are provided as follows, [20]

- Limit analysis
    - Enables to compute robust upper and lower bounds of collapse load
- Strength reduction analysis
    - Determination of strength based on the factor of safety
- Elastoplastic analysis
    - Suitable for staged constructions and SLS design. More details of this analysis are given in section 3.4.5
- Structural elements
    - Materials used for structural element simulation include shells, shear joints, and geogrids, among others.
- Mesh adaptivity
    - This tool enhances the mesh generation process automatically. More details of this feature are given in section 3.4.6.

The sign convention in Optum G3 is identical to that of the 2D version, and it utilizes a global cartesian coordinate system. [21]

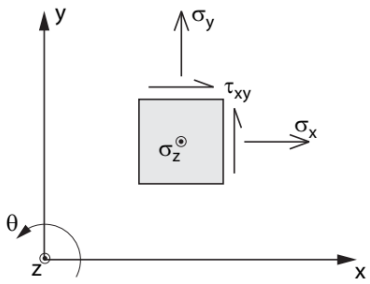

Figure 3-1: 2D Sign convention [21]

3.4.1 Limit analysis approach in Optum G3

In most cases, the primary objective of geotechnical engineers is to define the ultimate capacity of a foundation (ULS). In this case, with the use of the FELA approach, Optum G3 offers a single-step calculation to define the collapse load with the option to have the upper and lower bounds of the collapse load, allowing the user to check the accuracy of the result.

When finer meshes are generated, the gap between upper bound and lower bound solutions decreases, bringing the solution closer to the exact solution, as shown in Figure 3-2, where (a) represents the solutions with coarse meshes and (b) represents the solutions with finer meshes.

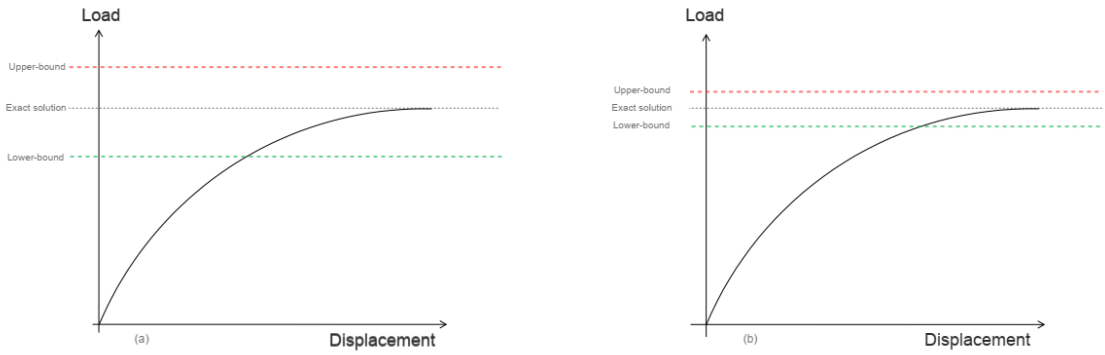

Figure 3-2: Interval of upper and lower bound solutions for different meshes

3.4.2 Governing equations

The geometry of the problem is shown in Figure 3-3 where α is a load multiplier and the traction acting on volume V is α**t.** Body forces acting on the volume V and boundary of S are denoted as **b**. Displacements are indicated for boundary S_u while traction t is specified for boundary S_σ.

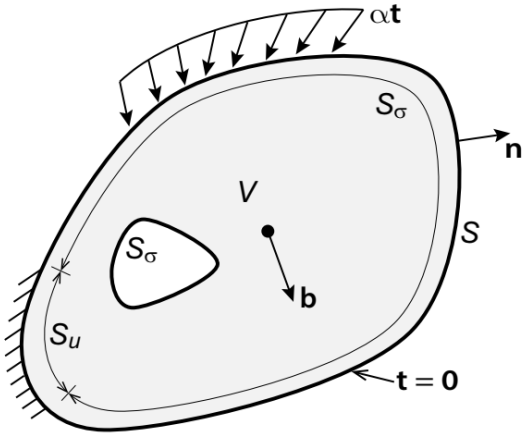

Figure 3-3: Solid with volume V and boundary of S subjected to tractions [19]

In general, stress at a point in three dimensions is defined as a six-dimensional stress vector,

$$\boldsymbol{\sigma} = \begin{Bmatrix} \sigma_x \\ \sigma_y \\ \sigma_z \\ \tau_{xy} \\ \tau_{yz} \\ \tau_{zx} \end{Bmatrix} \tag{3.1}$$

The static equilibrium equation for plane-strain (2D) condition is,

$$\begin{aligned} \frac{\partial \sigma_x}{\sigma_x} + \frac{\partial \tau_{xy}}{\sigma_y} + \mathrm{b}_x = 0 \\ \frac{\partial \sigma_y}{\sigma_y} + \frac{\partial \tau_{xy}}{\sigma_x} + \mathrm{b}_y = 0 \end{aligned} \tag{3.2}$$

Body forces $\mathbf{b} = \begin{Bmatrix} b_x \\ b_y \end{Bmatrix}$, above equation can be written in matrix form,

$$\begin{aligned} &\boldsymbol{\nabla}^T\boldsymbol{\sigma} + \boldsymbol{b} = \mathbf{0}, \quad \text{in V} \\ &\boldsymbol{\nabla}^T = \begin{bmatrix} \frac{\partial}{\partial_x} & 0 & 0 & \frac{\partial}{\partial_y} \\ 0 & \frac{\partial}{\partial_y} & 0 & \frac{\partial}{\partial_x} \end{bmatrix} \end{aligned} \tag{3.3}$$

The static boundary conditions can be described as follows,

$$\begin{aligned} n_x\sigma_x + n_y\tau_{xy} &= t_x \\ n_y\sigma_y + n_x\tau_{xy} &= t_y \end{aligned} \tag{3.4}$$

X and y components of traction vector $\mathbf{t}$ are defined as t_x and t_y and traction vector $\mathbf{n} = \begin{Bmatrix} n_x \\ n_y \end{Bmatrix}$ which is normal to the boundary.

The matrix form of the equation (3.4) can be written as follows,

$$\begin{aligned} &\mathbf{P}^T\boldsymbol{\sigma} = \alpha\mathbf{t}, \quad \text{acting on } S_\sigma \\ &\mathbf{P}^T = \begin{bmatrix} n_x & 0 & n_y \\ 0 & n_y & n_x \end{bmatrix} \end{aligned} \tag{3.5}$$

The conventional plasticity theorem is based on the decomposition of total strain into elastic and plastic parts,

$$\varepsilon = \varepsilon^e + \varepsilon^p \tag{3.6}$$

Where ε is total strain and ε^e and ε^p corresponds to elastic and plastic strain which are,

By introducing compliance modulus C elastic strain can be written as follows,

$$\varepsilon^e = C\boldsymbol{\sigma} \tag{3.7}$$

Plastic strain rate is shown on equation (3.8) where, $\dot{\lambda}$ is plastic multiplier and G is the flow potential.

A plastic strain occurs when $F(\sigma) = 0$, where the stress state is the yield state the condition satisfies equation (3.9),

$$\dot{\varepsilon}^{p} = \dot{\lambda}\frac{\partial G}{\partial \boldsymbol{\sigma}}, \qquad \dot{\lambda} \geq 0 \tag{3.8}$$

$$\dot{\lambda} F(\boldsymbol{\sigma}) = \mathbf{0} \tag{3.9}$$

Velocity field can be derived by the assumption of small strain,

$$\dot{\varepsilon}^{\mathrm{p}} = \boldsymbol{\nabla}\dot{\mathbf{u}} \tag{3.10}$$

The combination of equations (3.8) and (3.10),

$$\boldsymbol{\nabla}\mathbf{u} = \dot{\lambda}\frac{\partial G}{\partial \boldsymbol{\sigma}} \tag{3.11}$$

Yield condition requirement,

$$\mathrm{F}(\sigma) \leq 0 \tag{3.12}$$

Linearized yield function,

$$\mathbf{F}^{T}\boldsymbol{\sigma} - \mathbf{k} + \mathbf{s} = \mathbf{0}, \qquad \text{for } \mathbf{s} \geq \mathbf{0} \tag{3.13}$$

3.4.3 Lower bound FELA

According to [19], one way to define the governing equations is through the lower bound principle by maximizing load multiplier α,

$$\begin{aligned} \nabla^{\mathrm{T}}\boldsymbol{\sigma} + \mathbf{b} &= 0, \text{ in V} \\ \mathbf{P}^{\mathrm{T}}\boldsymbol{\sigma} &= \alpha\mathbf{t}, \text{on } S_{\sigma} \\ \mathbf{F}^{\mathbf{T}}\boldsymbol{\sigma} - \mathbf{k} + \mathbf{s} &= \mathbf{0}, \mathrm{s} \geq 0 \end{aligned} \tag{3.14}$$

The lower bound of the exact multiplier is defined by developing a stress field that satisfies the equilibrium, boundary, and yield conditions.

3.4.4 Upper bound FELA

Upper bound governing equations can be written as follows, the aim is to minimize the equation (3.15) which is subjected to equation (3.16),

$$\int_V \mathrm{k}^T \dot{\lambda} dV - \int_V \mathrm{b}^T \dot{u} dV \tag{3.15}$$

$$\nabla \dot{u} = F\dot{\lambda} \; for \;\; \dot{\lambda} \geq 0$$
$$\int_V \mathrm{t}^T \dot{u} dS = 1 \tag{3.16}$$

The problem needs kinematic quantities of velocity fields that satisfy the flow rule, which makes it possible to achieve the upper bound solution, displacement boundary conditions, associated flow rule, and strain displacement conditions should be satisfied. [19]

3.4.5 Elastoplastic analysis in Optum G3

The elastoplastic analysis is appropriate for situations where the deformations are concerned with a specific load, such as staged construction-related geotechnical problems like deep excavation and embankment construction. These types could be easily and precisely solved with Optum G3 using elastoplastic or consolidation analysis types. [22]

3.4.6 Adaptive mesh

The adaptive meshing tool will provide more accurate results by refining the meshes over regions that necessitate finer meshing, which would be based on the solution and will occur simultaneously during the calculation. The user can start with very coarse meshing and then use the adaptive meshing tool to refine or coarsen the meshes and calculate more accurate results. Any other geotechnical FE software does not have an adaptive mesh refinement tool. [23].
The influence of adaptive meshing on the towhead model is illustrated in section 4.1.3.

3.4.7 Flow rule effects

The angle of dilatation is assumed to be constant during plastic yielding and regulates the amount of plastic volumetric strain generated during plastic shearing. In many researches, it is suggested to take dilation angle ψ as φ -30 for non-cohesive soils with $\varphi > 30°$, however, this will lead to inaccurate results in ultimate capacity as shown on Figure 3-4. [24]

As previously discussed in section 3.2, the limit analysis assumes an associated flow rule. The associated flow rule has less effect on soil ultimate capacity but contributes more to displacement. As a result, the ultimate capacity of the foundation is independent of the flow rule. When the non-associated flow rule in the ultimate capacity analysis is assumed, there may be multiple limits loads each satisfying the governing equations, comparison is shown in Figure 3-4. [19]

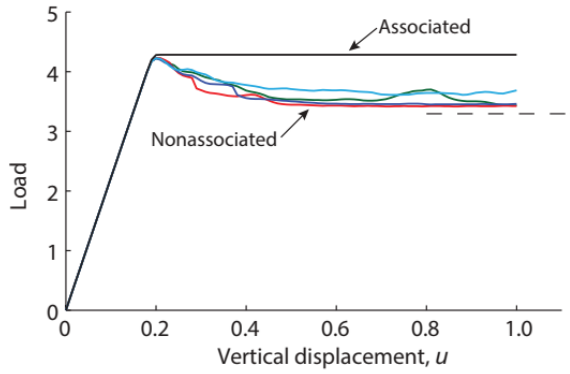

Figure 3-4: Load displacement curve for associated and nonassociated flow rule [19]

Another outcome of using a non-associate flow rule for ultimate capacity calculation is a significant decrease in limit load when compared to using an associated flow rule, the difference in friction and dilation angle determines the decrease in limit load for the Mohr-coulomb soil model, the two most likely causes of this discrepancy are,

- Influence of nonassociated flow in localization
- Allowance of flow rule to some limitations on the kinematics of shear bands.

Load P is acting on a rigid block shown in Figure 3-5, the aim is to find the maximum value for Q, according to Mohr-coulomb yield criteria, equation (3.17) can be written and followed by the flow potential G equation, where φ is the friction angle.

$$F = \sqrt{(\sigma_x - \sigma_y)^2 + 4\tau_{xy}{}^2} + (\sigma_x + \sigma_y) \cdot \sin\varphi \quad (3.17)$$

$$G = \sqrt{(\sigma_x - \sigma_y)^2 + 4\tau_{xy}{}^2} \quad (3.18)$$

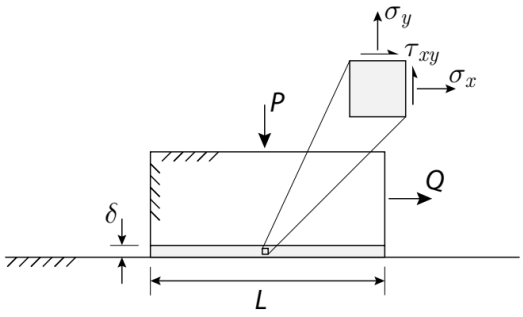

Figure 3-5: Rigid block on the frictional surface [19]

The above equation can be written by assuming

$$\sigma_x = \sigma_y \quad (3.19)$$

$$F = 2|\tau_{xy}| + 2\sigma_y \sin\varphi = 0 \quad (3.20)$$

From equation (3.20), Q can be written as follows,

$$Q = P \cdot \sin\varphi \quad (3.21)$$

The standard solution with the assumption of associated flow rule ($G = F$) from general Mohr-coulomb failure criteria ($\tau = \sigma \cdot \tan(\varphi) + c$) is written below,

$$Q = P \cdot \tan(\varphi) \quad (3.22)$$

The difference between two flow rules may be evaluated by introducing an effective friction angle, $\tan\varphi^* = sin\,\varphi$

$$Q = \mathrm{P} \cdot \tan(\varphi^*) \quad (3.23)$$

As an example, when $\varphi = 38°, \tan\varphi / \tan\varphi^* = 1.27$, which is comparable to the ratio of characteristic and design friction angle in code requirements

Throughout this thesis associated flow rule is considered for the Mohr-Coulomb sand model as the aim is to define the ultimate capacity of the towhead foundation.

3.5 Finite element analysis

Limit equilibrium was a widely used method to determine the stability of soil in geotechnical practices, however, this method does not satisfy all stress equilibrium equations and it is an approximate approach, also there is not any mechanism to check the final answer. [18]

Finite element analysis is quite different when compared to finite element limit analysis. To perform analysis with the displacement finite element method both strength and strain parameters should be known, unlike the limit analysis which can perform with only strength parameters. Models analyzed in this method are highly dependent on mesh and the number of load steps, so for accuracy check it is crucial to adjust the mesh adaptivity which can affect the limit load.

The following chapter introduces the fundamentals of Plaxis 3D software, which is based on the kinematic form of displacements. [25]

3.6 Utilized software for FEA

Plaxis 3D is a computer program that is designed for defining deformation, stability, and water flow among other features, it is based on finite element analysis (FEA) and is one of the most broadly used geotechnical engineering software program.

A summary of the most important features of Plaxis from [26] is provided below.

- Boreholes
    - Soil layers can be defined by the generation of boreholes, for inclined surfaces various boreholes can be defined, Plaxis propagates layers and ground surface locations between boreholes automatically.
- Mesh generation
    - Plaxis allows users for automatic generation of meshes, also there are options to refine the local meshes manually. More details are given in chapter 3.6.1.
- Interfaces
    - Interfaces may use for simulation of soil-structure interaction where the strength parameters may not be the same as the adjacent soil layer.
- Loads
    - There are several types of loading in Plaxis, namely, fixed point load, line loads, and distributed loads.
- Mohr-Coloumb model
    - A simple and non-linear MC model is based on soil parameters that are known in most practical cases, it is commonly used for determining of ultimate bearing capacity of foundations.
- Hardening soil model
    - This model allows for plastic compaction along with plastic shearing, it is commonly used in cases that involve loading and unloading of soil, as the soil's unloading characteristic is accounted for in this model.
- Structural elements
    - These elements possess linear elastic behavior, which applies to beams, walls, and plates.
- Staged construction
    - Plaxis can simulate staged construction by activating and deactivating various elements for each stage.
- Presentation of the outputs
    - The computed results, as well as deformed meshes and geometry, can be displayed in a variety of graphs and curves.

The software uses a cartesian coordinate system, therefore all compressive stresses and forces are negative, whereas tensile stresses and forces are positive. [27]

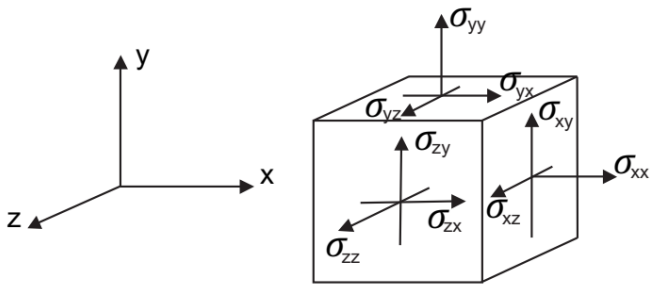

Figure 3-6: Sign convention [27]

Plaxis 3D features a variety of soil and structural elements. The fundamental soil element in the 3D version is a 10-node tetrahedron, as seen in Figure 3-7

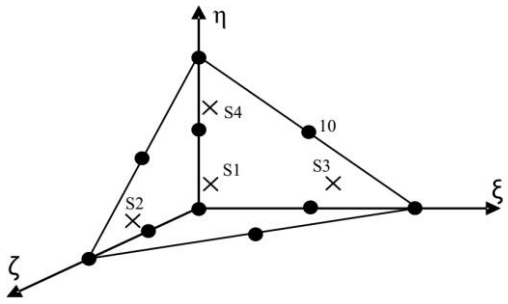

Figure 3-7: 10-node tetrahedron element [27]

Also, the elements used to perform the structural behavior of beams, plates, and interfaces are as follows,

- 3-node linear beam elements
- 6-node plate and geogrid elements
- 12-node interface elements

Boundary conditions are set to default by Plaxis and it is possible to change it as well. By default, the model is fixed at the bottom in all directions, the top surface is free and vertical sections are fixed in the horizontal direction, as you can see in Figure 3-8 below.

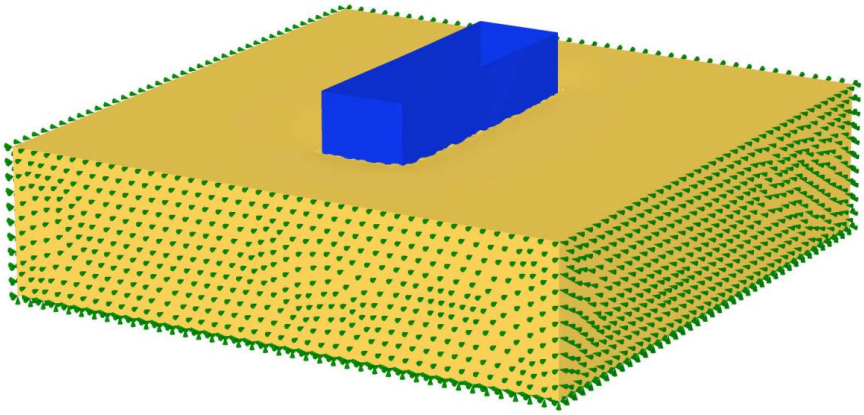

Figure 3-8: Boundary conditions

3.6.1 Mesh generation

After creating the model in Plaxis, in order to apply the finite element method, the geometry should be divided into smaller pieces, which is called mesh generation, generated smaller meshes will connect by nodes. There is not any adaptive meshing option in Plaxis 3D instead there are predefined mesh sizes that vary from very coarse to very fine. As previously mentioned, the accuracy of the model in this report is highly dependent on several elements thus finer the mesh, the more accurate the result, however, running the model with many elements may take a long time because it requires high-end computers.

Chaper 4: Results of numerical analysis

This section presents all the results of the analysis from Optum G3 and Plaxis 3D. Results of hand calculation are presented in the appendices section of this report.

4.1 Optum G3

4.1.1 The geometry of the model

As shown in Figure 4-1, the soil domain is 50 x 50 meters in size with a depth of 10 meters. Trawl load and weight of structure assigned as fixed loads and multiplier load applied beneath

the footing. The model is also fixed in all directions at the bottom, with the top surface free and vertical sections fixed in the horizontal direction, by applying standard fixities.

Dimensions of soil domain and towhead foundation are shown in Table 4-1.

Table 4-1: Soil domain and towhead dimensions – Optum G3

	X_{min}	X_{max}	Y_{min}	Y_{max}	Z_{min}	Z_{max}
Towhead Foundation	-10 m	10 m	-3 m	3 m	0	4.5 m
Soil Domain	-25 m	25 m	-25 m	25 m	-10 m	0

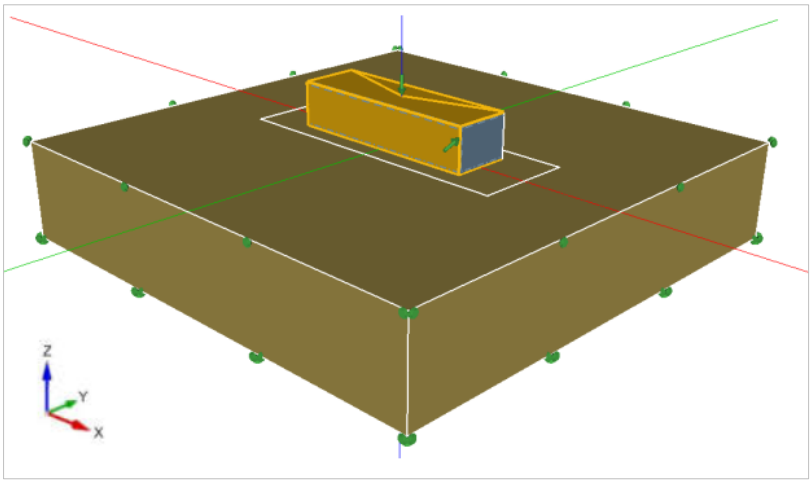

Figure 4-1: Geometry and soil domain

4.1.2 Soil properties and interfaces

Towhead mass is modeled as a rigid solid and to apply self-weight and trawl load to rigid elements in Optum G3, interfaces must be applied, both x-z and x-y planes introduced with shell element.

Interface with a reduction factor of 0.87 for soil and steel contact area assigned to lower the friction angle in soil-structure interaction, resulting in a reduced φ of around 33˚.

Sand model properties are shown in Table 4-2

Table 4-2: Input soil properties

Soil type	Sand	-
Soil model	Mohr-Coulomb	-
Drainage type	Drained	-
Unit weight (saturated)	9,5	kN/m^3
Unit weight (unsaturated)	9,5	kN/m^3
Soil-structure interface reduction factor	0.87	-

4.1.3 Mesh generation

Figure 4-2 shows created meshes to demonstrate the capability of the adaptive meshing tool. (a) is generated meshes with an adaptive meshing tool, and (c) is an x-y plane view that illustrates how the finer meshes surrounding the towhead foundation area where the applied loads have an effect. Comparably, (b) and (d) illustrate mesh volume created without adaptive meshing tool, resulting in the same mesh sizes across the geometry. Also, additional soil volume is created to facilitate the mesh refining process.

In Optum G3, there are three types of elements, lower, upper and mixed. The model is analyzed using the mixed element type, which is a combination of lower and upper bound elements.

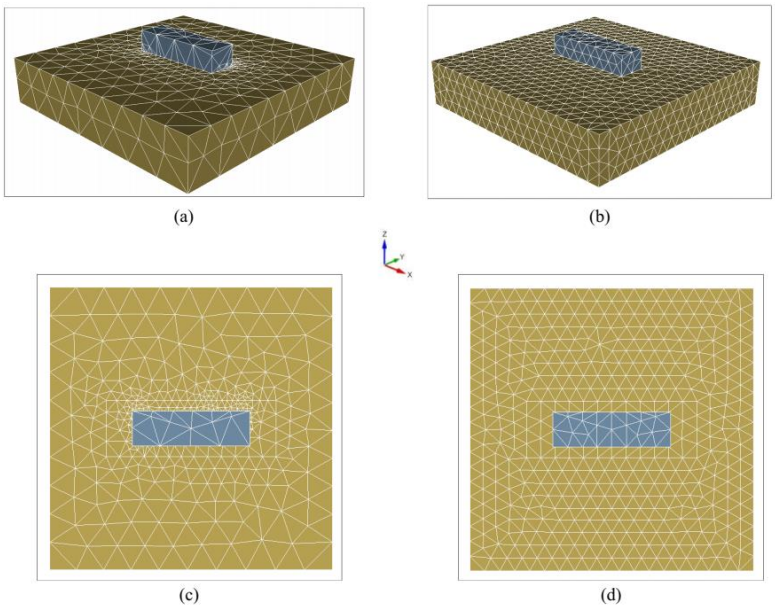

Figure 4-2: Mesh generation with 10.000 elements

4.1.4 Results

The analysis was completed in a single calculation by applying trawl load as fixed 661 kN with 20˚ inclination, another fixed load for the trial weight of towhead entered as 2000 kN with multiplier load, therefore the minimum weight of the towhead is calculated as 2340 kN.

The model is calculated with 1000 elements initially, with upper bound, lower bound, and mixed type elements, as shown in Figure 4-3 . As the element numbers increase to roughly 12000, the solutions of mixed element converge to 2340 kN.

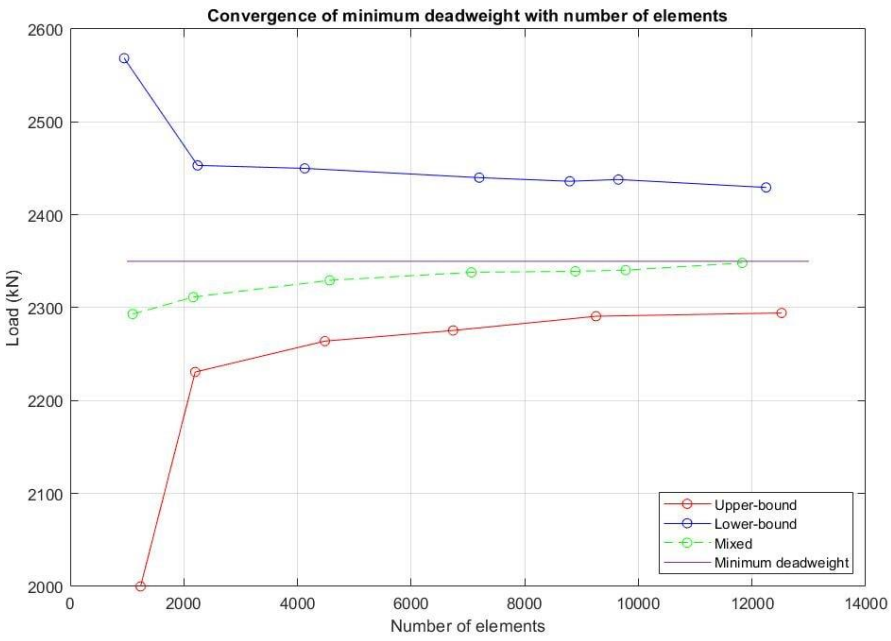

Figure 4-3: Convergence of load with different element sizes

The failure mechanism of the towhead is illustrated in Figure 4-4 and it is sliding with small bearing failure on the surface, to have a better perspective of the failure mode, x-y, and y-z plane sections are added to parts (c) and (d) of Figure 4-4.

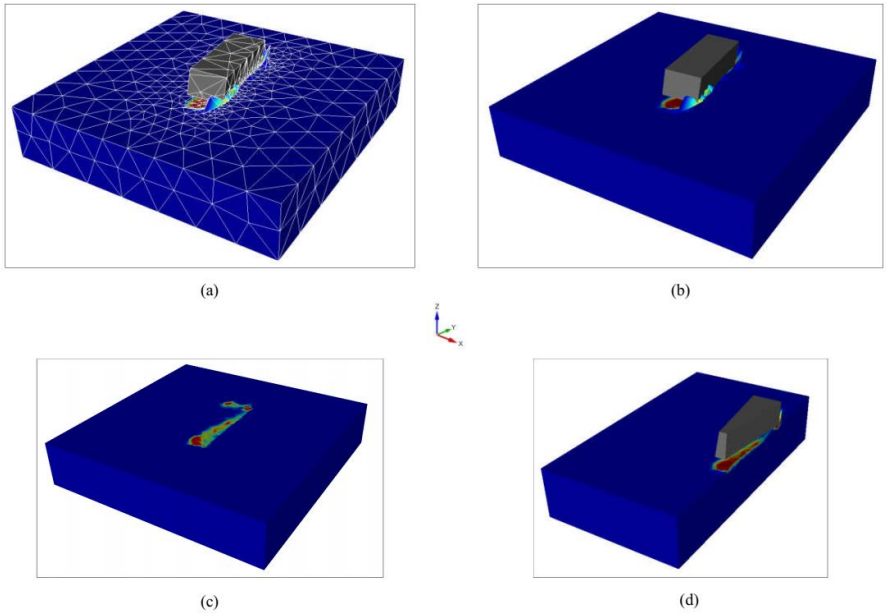

Figure 4-4: Failure mechanism of towhead

4.2 Plaxis 3D

This section of the report will use the Plaxis 3D 2022 version to illustrate the ultimate bearing capacity of towhead model under self-weight and trawl load by using the conventional finite element approach.

4.2.1 The geometry of the study

The geometry of the problem is identical to the Optum G3. Towhead is modeled as a rectangular box with dimensions of 20 meters long, 6 meters wide, and 4.5 meters high. The trawl load acts on the top corner of the structure with a 20° inclination.

Table 4-3 shows the dimensions of the soil domain and the towhead foundation. Those dimensions are also illustrated in Figure 4-5.

Table 4-3: Soil domain and towhead dimensions – Plaxis 3D

	X_{min}	X_{max}	Y_{min}	Y_{max}	Z_{min}	Z_{max}
Towhead Foundation	-3 m	3 m	-10 m	10 m	0	4.5 m
Soil Domain	-20 m	20 m	-20 m	20 m	-10 m	0

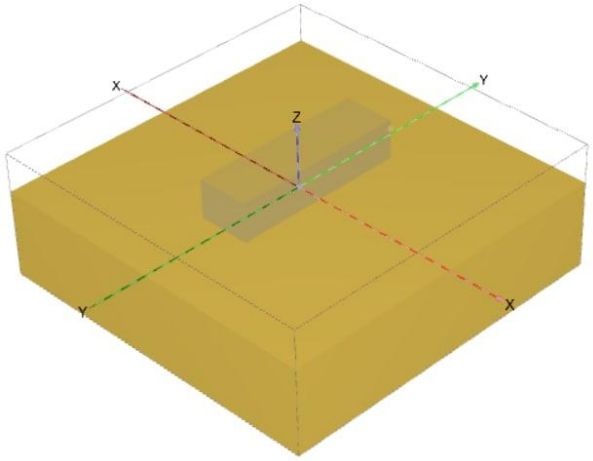

Figure 4-5: Plaxis 3D model of towhead on soil domain

4.2.2 Input materials

The soil beneath the towhead is assumed to be sand with the Mohr-Coulomb failure criterion. Towhead is modeled using the Plaxis plate element as an elastic material. Table 4-4 and Table 4-5 show all of the input data for the soil and plate elements. The interface has been assigned as a new material with the same properties as Mohr-Coulomb sand, with the exception that the friction angle has been reduced to 33° with strength reduction, R_{inter} has been set to 1.00, and gap closure left unselected.

Table 4-4: Soil model properties

Soil type	Sand	-
Soil model	Mohr-Coulomb	-
Drainage type	Drained	-
Unit weight (saturated)	9,5	kN/m^3
Unit weight (unsaturated)	9,5	kN/m^3
E'_{ref}	5000	kPa
C'_{ref}	0,1	kPa
Internal friction angle (φ)	38	Degree
Dilation angle (ψ)	38	Degree

Table 4-5: Plate properties

Plate type	Steel Plate	-
Material type	Elastic	-
Unit Weight	0	kN/m3
Young's modulus (E)	2,10E+08	kN/m2
Plate Thickness	0,3	m

4.2.3 Mesh Generation of the model

To illustrate the different meshes and element numbers, Table 4-6 and Figure 4-6 are presented. The coarseness factor is predefined as 1.00 for the soil domain and 0.5 for structural elements. Moreover, rather than using predefined mesh sizes, the user could also change the predefined coarseness factor of the desired volume.

Table 4-6: Number of elements and nodes for different element distribution

Case	Element Distribution	Number of Elements and nodes	Number of nodes
a.	Very coarse	1.489	2.956
b.	Coarse	2.953	5.147
c.	Medium	6.436	11.672
d.	Fine	15.835	26.861
e.	Very fine	37.838	61.365

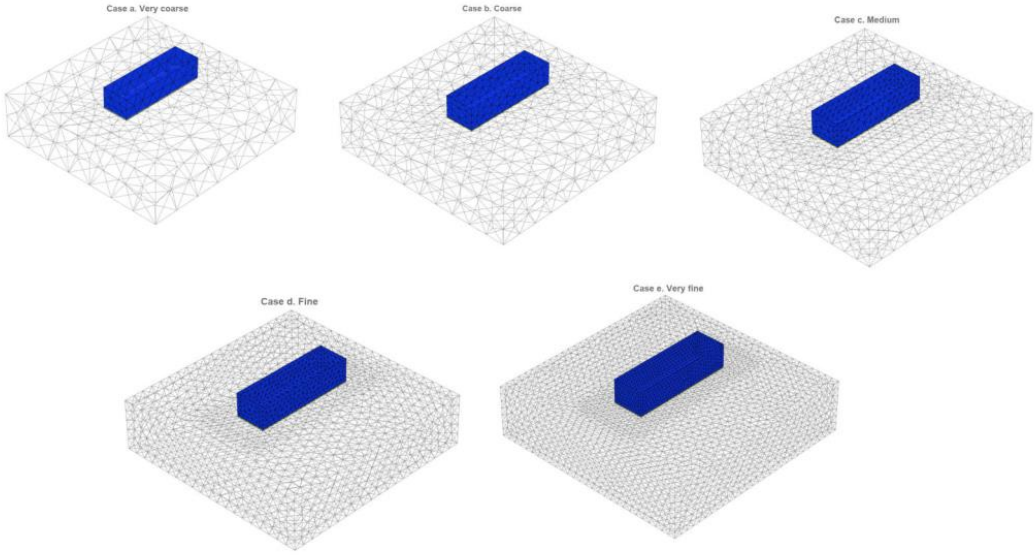

Figure 4-6: Plaxis 3D Different mesh generation with predefined patterns

After creating the model, the predefined meshing system presented earlier was revised so that instead of generating meshes with predefined patterns, the model was generated with a different coarseness factor. In addition, the soil volume around the towhead foundation was defined for strengthening the mesh refinement. As shown in Figure 4-7, the entire analysis in this report was completed with 36.804 elements and 57.955 nodes.

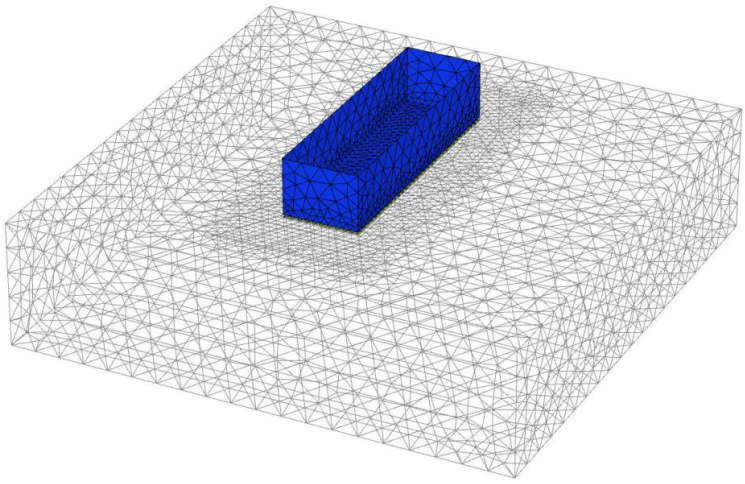

Figure 4-7: Mesh generation and refinement around the foundation

4.2.4 Point selection for curve generation

To construct all of the necessary curves in Plaxis 3D, the user must define a point before starting the calculation step, in this report, the point under trawl load with coordinates of (3, 10, and 0) is chosen. (Figure 4-8)

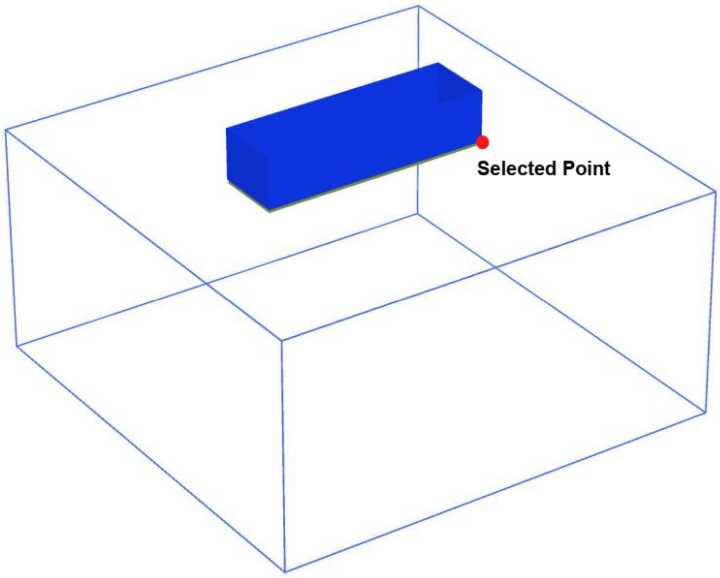

Figure 4-8: Selected point for curve generation

4.2.5 Results

To determine the towhead's minimum weight, the analysis started with a guess of towhead weight and gradually reduced it until failure, with each calculation performed independently for each loading scenario.
The towhead weight was initially set at 3100 kN and gradually reduced within 5 load scenarios (Table 4-7), with the trawl load remaining constant for all loading cases.

Loading coordinates are shown in Table 4-8, where the components of 661 kN of trawl load are taken in the x and y directions using the sign convention.

Table 4-7: Load cases

Case-1	3100 kN Deadweight
Case-2	2800 kN Deadweight
Case-3	2600 kN Deadweight
Case-4	2400 kN Deadweight
Case-5	2350 kN Deadweight
Case-6	2200 kN Deadweight

Table 4-8: Loading coordinates

X [m]	Y [m]	Z [m]	F_x [kN]	F_y [kN]	F_z [kN]
3,00	10,00	3,50	-621,10	0,00	226,10
0,00	0,00	0,00	0,00	0,00	-3100

Each case was estimated using different deadweights, and followed by a 200-step safety analysis to determine the factor of safety for each loading case. The towhead model failed with a deadweight of 2200 kN in the last load case, hence the least possible weight for towhead is computed as 2350 kN with a 1.03 factor of safety. The load-displacement curves for each load case are displayed in Figure 4-9.

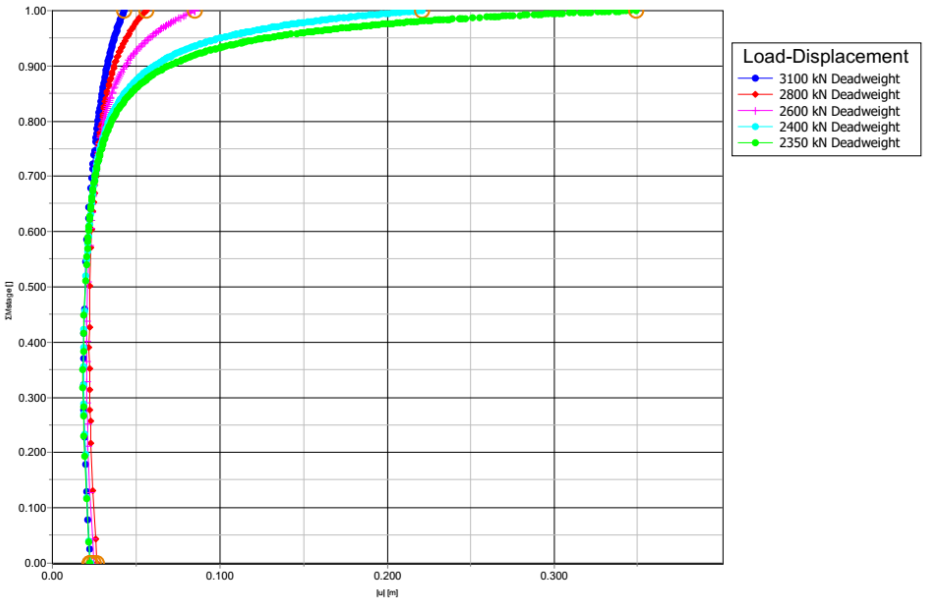

Figure 4-9: Load-displacement curve for all cases

Plaxis 3D's output panel allows users to see stress fields, deformed meshes, displacements, and more. Meshes will be displaced as a result of the applied loads, which help the user identify the

failure mechanism. Figure 4-10 shows the towhead failure mechanism as sliding with slight bearing failure at the surface.

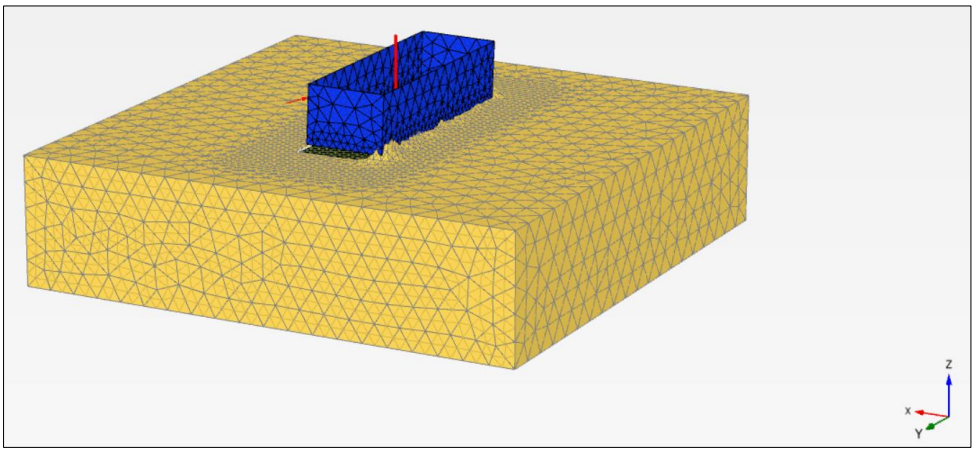

Figure 4-10: Deformed mesh with 2350 kN vertical load and trawl load

As shown in Figure 4-11 the shear stress distribution on the surface of the footing is not uniform, and it achieved its maximum value at the opposite corner of the trawl load, as expected.

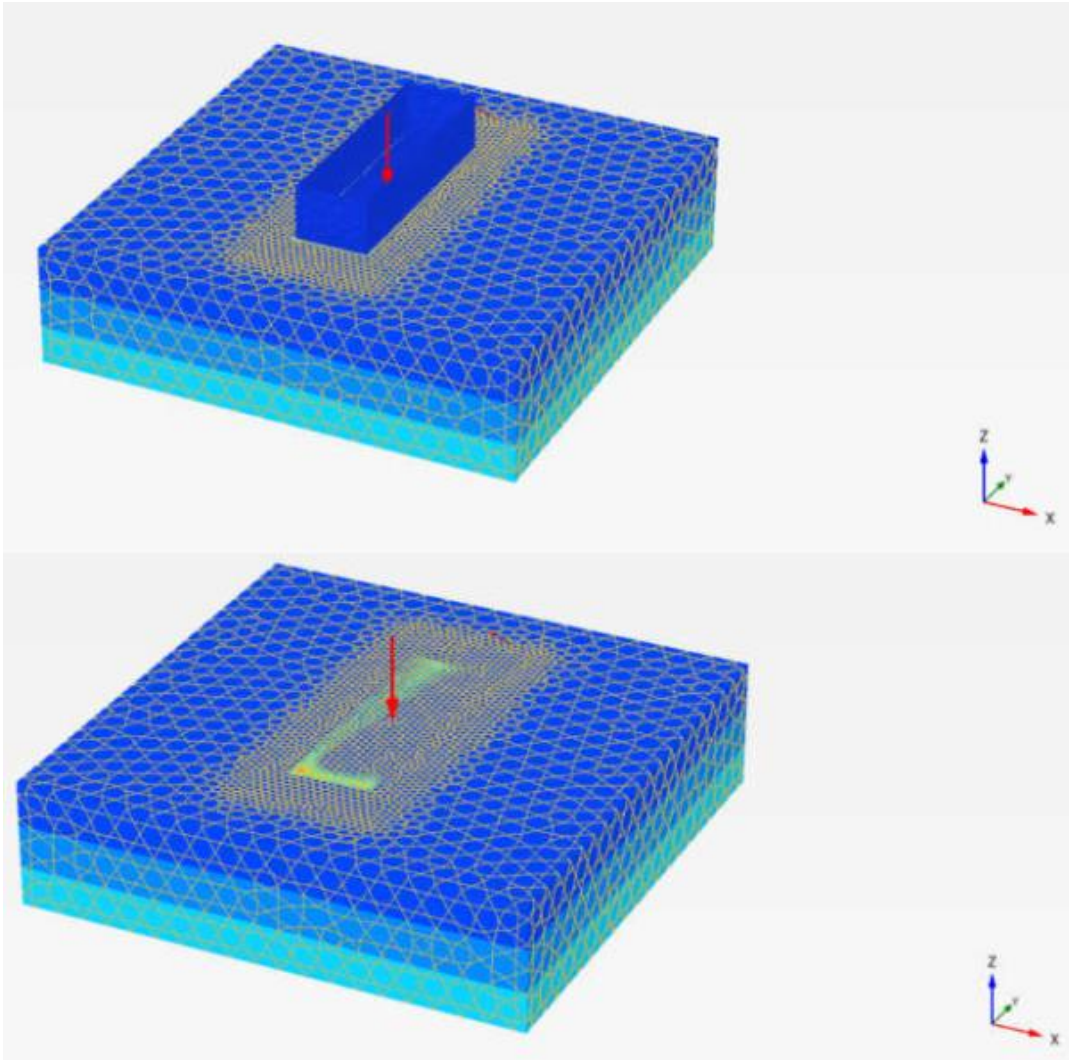

Figure 4-11: Shear stress distribution

Figure 4-12 and Figure 4-13 show the incremental displacements of meshes under vertical and horizontal towhead loading. These figures demonstrate that the displacements are shallow.

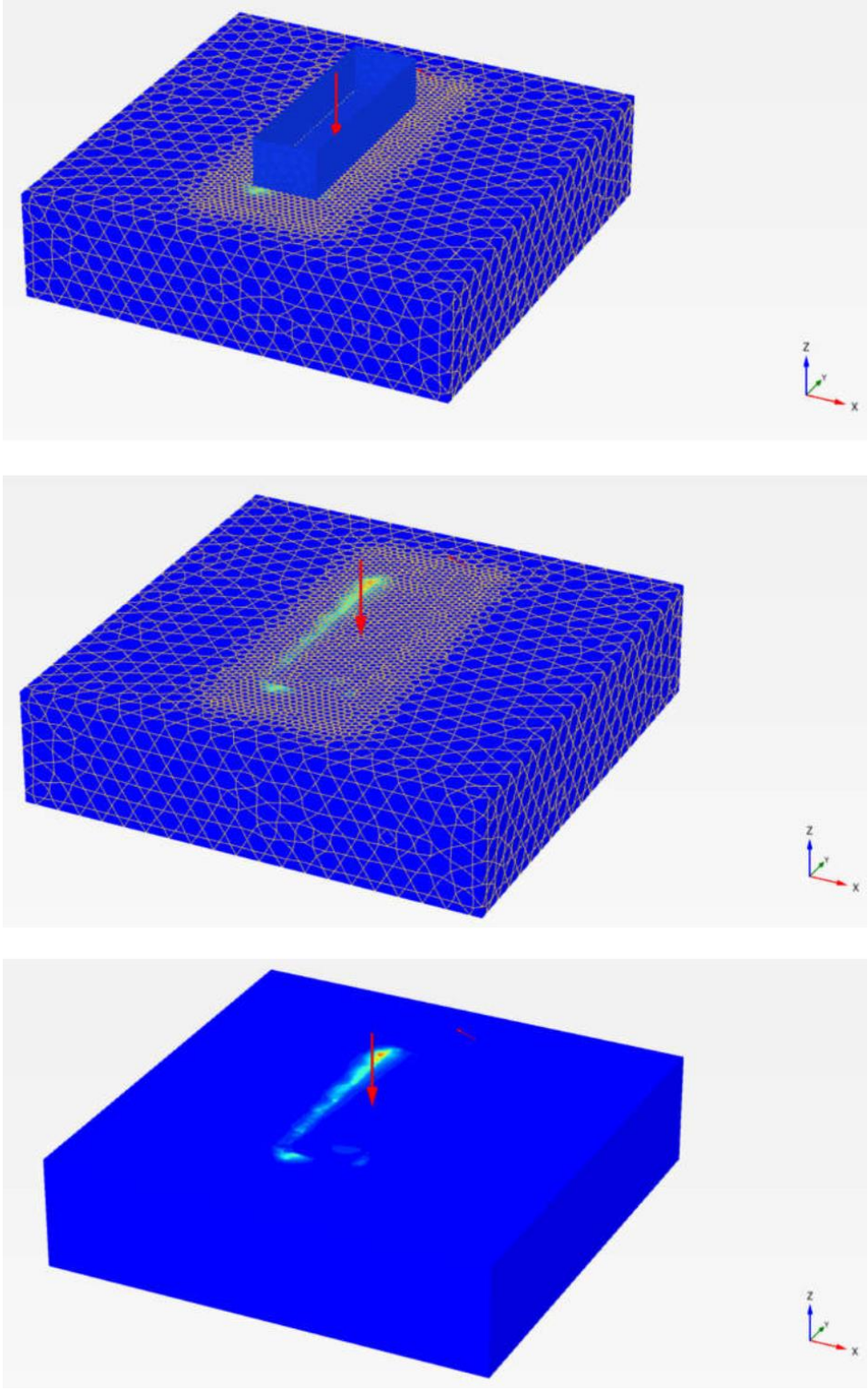

Figure 4-12: Incremental displacement

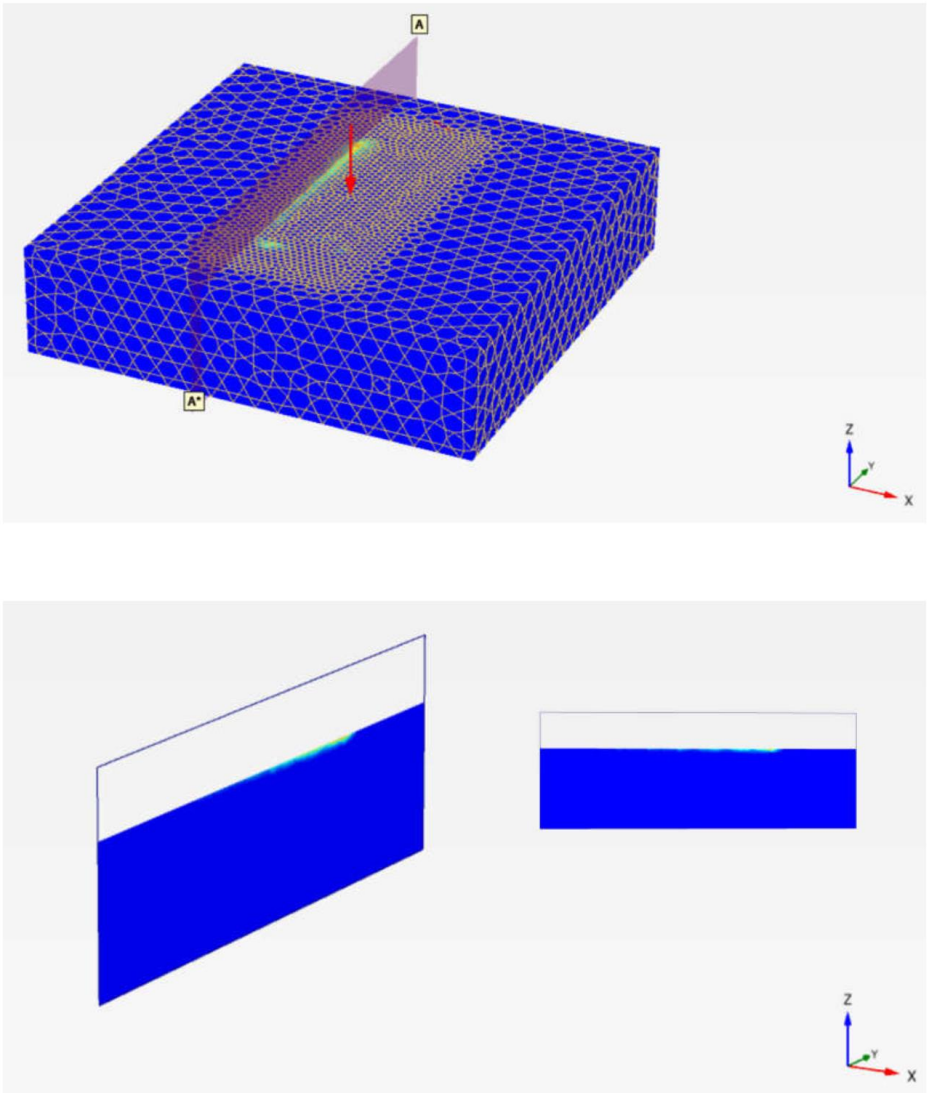

Figure 4-13: Cross-sections of incremental displacement

Chaper 5: Discussion of the results

Three different approaches were used to calculate the towhead minimum weight in the presence of trawl load, namely,

- FELA approach with Optum G3
- FEA approach with Plaxis 3D
- The analytical solution according to DNV is given in the appendices part of this thesis.

Figure 5-1 gives a summary of the results.

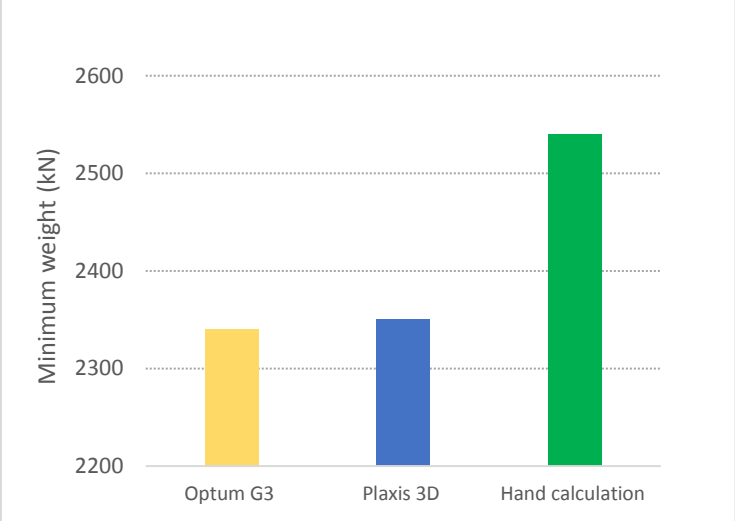

Figure 5-1: Summary of the results

It has been shown that Optum G3 is capable of calculating ultimate bearing capacity in a single calculation with strength parameters only, However, in analysis with Plaxis 3D, several calculation steps should be done with the knowledge of strength and strain parameters to find the minimum weight of towhead.

The limit analysis approach allows to check the accuracy of the failure load with consideration of upper and lower bound solutions, whereas the traditional method requires increasing the number of elements and thus finer the meshes which are considerably time-consuming and useless, as the aim of this thesis was to define the ultimate capacity of towhead rather than displacements.

The amount of time spent on numerical processes differed significantly between the two software. After determining the geometry, loads, and soil properties, the minimum weight with Optum G3 was obtained with a single calculation, but for Plaxis 3D it was calculated with six independent load cass. It is important to note that all of the analysis in this thesis were performed with the same computer. This considerable run time difference could be the bold outcome of this thesis, which was the main intention of using finite element limit analysis and demonstrating that this approach will save a significant amount of time in ultimate bearing capacity studies.

Previously, in section 2.3.2, in conventional approach, it is assumed that shear stress distributes evenly across the bearing area, but numerical analysis results showed that it tends to reach the maximum value on top corners with uneven distribution (Figure 4-11). The reason for this could be that conventional ultimate bearing capacity approach is based on the plane strain method.

Finally, a comparison of different approaches in the construction of the VH diagram can be seen in Figure 8-1, which was done by Optum CE [28], the model is the same as the one implemented in this study, a shallow foundation on the sand with drained condition. The comparison shows how the FELA approach fulfills the sliding limit. For the towhead model of this thesis, the same comparison between DNV and FELA is done with the scripting option of Optum G3, VH diagram for roughly 50 loading points have done in a couple of hours. As shown in Figure 8-2, the results for this study case are consistent.

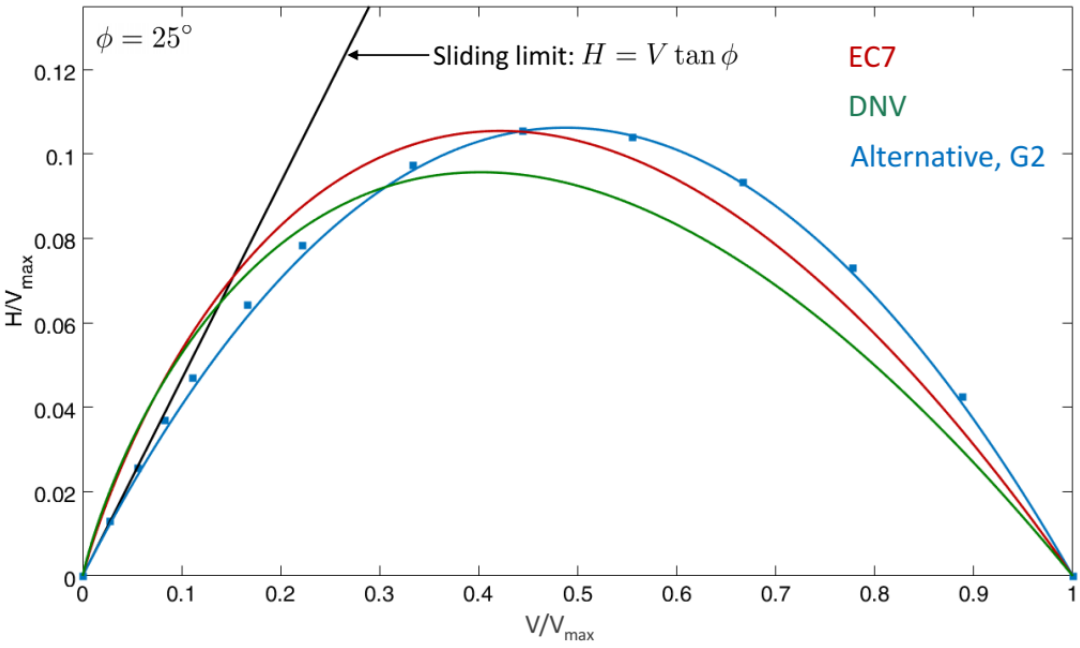

Figure 5-2: Comparison of HV diagrams [28]

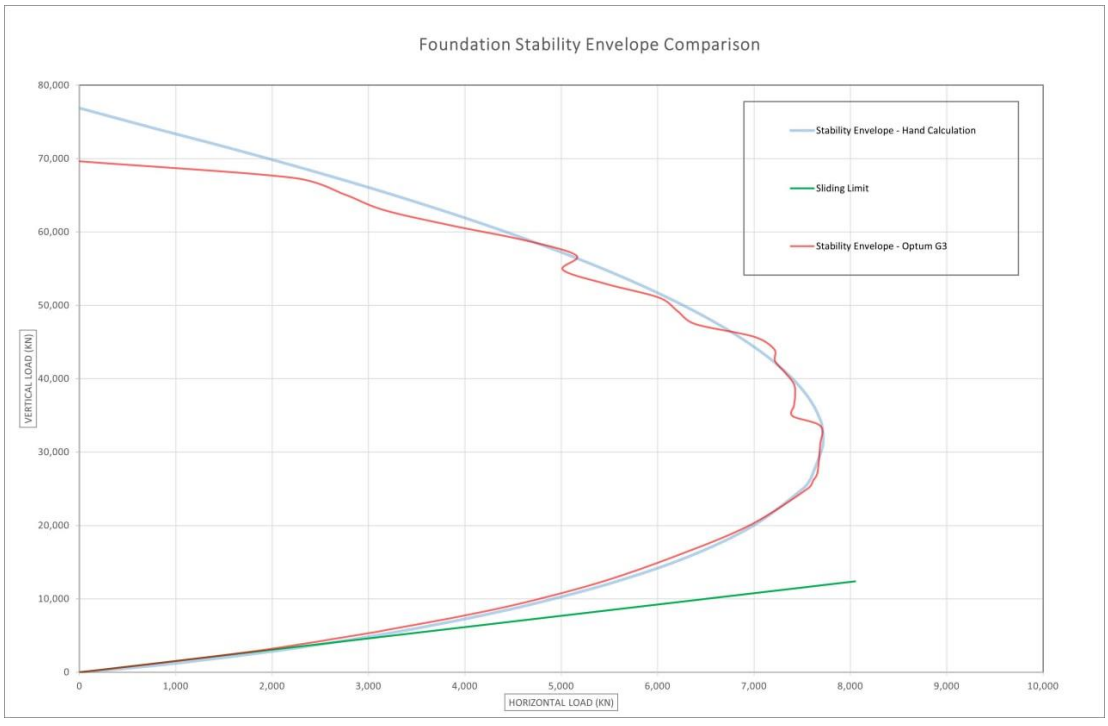

Figure 5-3: Foundation stability envelope derived by Optum G3 and hand calculations according to DNV

Chaper 6: Conclusion and recommendation for future works

6.1 Conclusion

The ultimate bearing capacity of a towhead foundation was investigated in this thesis by using finite element limit analysis and the conventional finite element method. The finite element limit analysis method was evaluated on Optum G3 software and compared to Plaxis 3D which is a strain element-based software.

The ultimate capacity of a towhead structure resting on sand with dimensions of 20x6 and 4.5 m. height was defined in the presence of trawl load, which causes a torsional moment on the foundation. Geometry, soil properties, and loading scenarios were all the same for the Optum G3 and Plaxis 3D analyses, as well as the hand calculations.

Even though 3D FELA is not a new analysis method, previous configurations were limited to simple cases with a maximum of 6000 elements. This thesis, on the other hand, demonstrates that FELA can solve complex geometries with asymmetric planes, which can be simulated with 60.000 elements if necessary. [29]
FELA approach with adaptive meshing tool has been demonstrated previously, with the presence of this tool, mesh generation was performed without modifying any coarseness factor by refining the meshes over regions that require finer meshes.

All in all, it can be concluded that finite element limit analysis is a strong tool to investigate the ultimate bearing capacity and it allows to save time and provides accurate solutions.

6.2 Recommendation for future works

The following areas for future research could be suggested,

- Towhead foundation of this thesis considered sand with the drained condition, future research could be done for clays or layered clay and sand in undrained condition.
- Consideration of seismic loads, which was not the case for this thesis.

Chaper 7: References

[1] DNV, "DNV-RP-C212 Offshore soil mechanics and geotechnical engineering. Recommended Practice," DNV, Oslo, Norway, Standard, Edition 2019. [Online]. Available: https://www.dnv.com/oilgas/download/dnv-rp-c212-offshore-soil-mechanics-and-geotechnical-engineering.html

[2] I. Green, "Subsea7 Innovation and Technology," p. 55, 2017.

[3] G. Wallace, "Subsea 7 towheads in Wick," 2014. https://commons.wikimedia.org/wiki/File:Subsea_7_towheads_in_Wick_%2815024767520%29.jpg

[4] C. Olsen, M. Kahlström, and T. Powell, "Bundle Towhead Foundation Design on Rock Berm Installed on Soft Clay," p. 9, 2016.

[5] P. R. Nystrøm, "Petroleum Safety Authority Study, NCS Trawl Development Study," p. 58, 2019.

[6] A. S. Vesic, "Analysis of Ultimate Loads of Shallow Foundation," 1973.

[7] B. M. Das, *Principles of foundation engineering*, Eighth edition/SI edition. 2014.

[8] G. G. Meyerhof, "THE ULTIMATE IBARING CAPACITY OF FOUNDATIONS," p. 32, 1951.

[9] B. M. Das , *Principles of geotechnical engineering*. Stamford, Conn.: Cengage Learning, 2010.

[10] J. B. Hansen, "A REVISED AND EXTENDED FORMULA FOR BEARING CAPACITY," p. 21, 1970.

[11] J. E. Bowles, E. P., and E. S., *Foundation Analysis and Design*. New York: McGraw-Hill, 1996.

[12] R. L. Michalowski, "An Estimate of the Influence of Soil Weight on Bearing Capacity Using Limit Analysis," *Soils Found.*, vol. 37, no. 4, pp. 57–64, Dec. 1997, doi: 10.3208/sandf.37.4_57.

[13] S. Krabbenhoft, L. Damkilde, and K. Krabbenhoft, "Lower-bound calculations of the bearing capacity of eccentrically loaded footings in cohesionless soil," *Can. Geotech. J.*, vol. 49, no. 3, pp. 298–310, Mar. 2012, doi: 10.1139/t11-103.

[14] C. Tang, K.-K. Phoon, and K.-C. Toh, "Effect of footing width on Nγ and failure envelope of eccentrically and obliquely loaded strip footings on sand.," *Can. Geotech. J.*, vol. 52, no. 6, pp. 694–707, Jun. 2015.

[15] Huang and Yu, *Foundation Engineering Analysis and Design*. 2018. [Online]. Available: https://doi.org/10.1201/9781351255400

[16] B. Hansen, *Geoteknik og fundering del II: Laboratoriet for Fundering, Danmarks Tekniske Højskole*. Den private ingeniørfond ved Danmarks tekniske Højskole, 1978. [Online]. Available: https://books.google.co.uk/books?id=P5x1XwAACAAJ

[17] C. Olsen, "Resurrection of the Limit Analysis in Geotechnical Design," 2019.

[18] S. Sloan, "Geotechnical stability analysis," *Géotechnique*, vol. 63, pp. 531–572, Jun. 2013, doi: 10.1680/geot.12.RL.001.

[19] K. Krabbenhoft, A. Lyamin, and J. Krabbenhoft, "OptumG2: Theory," 2016.

[20] K. Krabbenhoft, A. Lyamin, and J. Krabbenhoft, "OptumG2: Examples," 2016.

[21] K. Krabbenhoft, A. Lyamin, and J. Krabbenhoft, "OptumG2: Materials," 2016.

[22] K. Krabbenhoft, A. Lyamin, and J. Krabbenhoft, "OptumG2: Analysis," 2016.

[23] K. Krabbenhoft, A. Lyamin, and J. Krabbenhoft, "OptumG2: Features," 2016.

[24] C. Olsen, "Geotechnical Engineering," 2020. http://www.colsen.dk/

[25] Plaxis 3D, "Plaxis 3D Scientific Manual," 2021, [Online]. Available: https://communities.bentley.com/cfs-file/__key/communityserver-wikis-components-

files/00-00-00-05-58/PLAXIS3D_2D00_CE_2D00_V22.00_2D00_2_2D00_Reference.pdf
[26] R. B. J. Brinkgreve and W. Broere, “PLAXIS 3D - GENERAL INFORMATION,” p. 17, 2004.
[27] Plaxis 3D, “Plaxis 3D Reference Manual,” 2020, [Online]. Available: https://communities.bentley.com/cfs-file/__key/communityserver-wikis-components-files/00-00-00-05-58/PLAXIS3D_2D00_CE_2D00_V22.00_2D00_2_2D00_Reference.pdf
[28] K. Krabbenhoft, *Optum CE Webinar: The Bearing Capacity Equation*, (2020). [Online Video]. Available: https://optumce.com/Download/Webinars/2020-05-14-Torsion.pdf
[29] H. P. Dunne, “Finite element limit analysis of offshore foundations on clay,” University of Oxford, 2017. [Online]. Available: uk.bl.ethos.748864

Chaper 8: Appendices

8.1 Hand calculations

Hand calculations for the effective area and interaction diagrams will be presented in this chapter which have done according to DNV.

8.1.1 The effective area of foundation

Towhead dimension is 20x6x4.5 m height, trawl load is acting with 20° inclination at top corner. All the acting forces are transferred to the foundation base. The coordinate system and a schematic sketch of the towhead can be seen in Figure 8-1

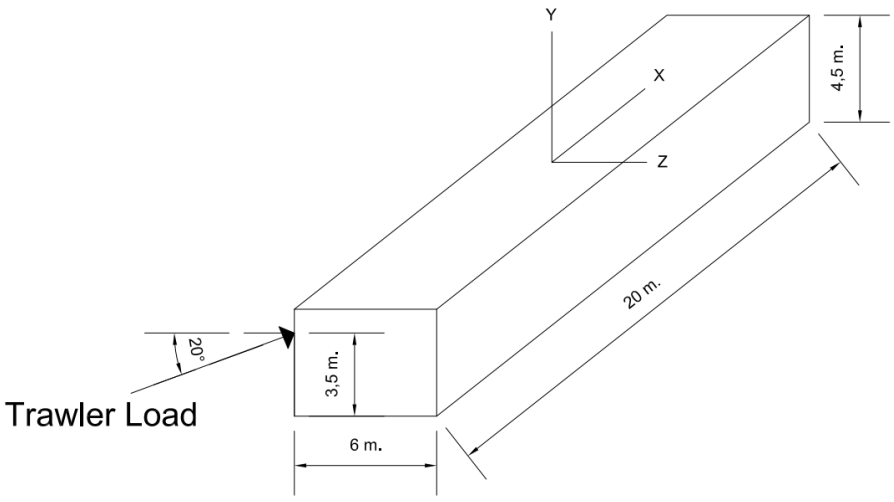

Figure 8-1: Towhead model dimension and trawl loading

The soil is assumed to be sand, with a unit weight of 9.5 kN/m^3 and internal friction angle of 38°. A trawl load of 661 kN acts on the top corner. In the first step of the analysis, a weight of 2000 kN was assumed for the towhead structure.

Loads acting on towhead;

$f_x = 0$

$f_y = 661 \cdot \sin 20^\circ = 226{,}1 \text{ kN}$

$f_z = 661 \cdot \cos 20^\circ = 621{,}1 \text{ kN}$

$w = 2000 \text{ kN}$ Assumed weight of towhead

$p = -2000 + 226{,}1 = -1773{,}9 \text{ kN}$

Distances to geometric center of towhead are as follows,

$x = 10 \text{ m}$

$y = 3.5 \text{ m}$

$z = 3 \text{ m}$

Moments acting on geometrical central of towhead,

$M_x = f_z \cdot y + f_y \cdot z = 621{,}1 \cdot 3{,}5 + 226{,}1 \cdot 3 = 2852{,}20 \text{ kN.m}$

$M_y = f_z \cdot x + f_x \cdot z = 621{,}1 \cdot 10 = 6211{,}37 \text{ kN.m}$

$M_z = f_y \cdot x + f_x \cdot z = -226{,}1 \cdot 10 = -2261 \text{ kN.m}$

Eccentricity in the x and z-axis calculated according to Equations (2.43) and (2.44),

$$e_x = \frac{M_z}{P} = \frac{-2261}{-1773{,}9} = 1{,}27 \text{ m}$$

$$e_z = \frac{M_x}{P} = -\frac{2852{,}20}{-1773{,}9} = -1{,}61 \text{ m}$$

Effective length and width of foundation calculated from Equations (2.45) and (2.46),

$l_{eff} = l - 2 \cdot |e_x| = 20 - 2 \cdot 1{,}27 = 17{,}45 \text{ m}$

$b_{eff} = b - 2 \cdot |e_z| = 6 - 2 \cdot 1{,}61 = 2{,}78 \text{ m}$

$A_{eff} = b_{eff} \cdot l_{eff} = 2{,}78 \cdot 17{,}45 = 48{,}59 \text{ m}^2$

A moment in the y-axis is recalculated because of the eccentricity,

$M_y = f_x \cdot e_z + f_z \cdot e_x = 0 + 621{,}1 \cdot (1{,}27) = 788{,}797 \text{ kN.m}$

$M_y = 6211{,}37 - 788{,}797 = 5419{,}77 \text{ kN.m}$

The equivalent horizontal load is defined by equation (2.49),

$$H = \sqrt{(f_x^2 + f_z^2)}^2 = 621{,}1\ \text{kN}$$

$$H' = \frac{2 \cdot M_y}{l_{eff}} + \sqrt{H_d^2 + \left(\frac{2 \cdot M_y}{l_{eff}}\right)^2} = \frac{2 \cdot 5419{,}77}{17{,}45} + \sqrt{621{,}1^2 + \left(\frac{2 \cdot 5419{,}77}{17{,}45}\right)^2} = \mathbf{1499{,}55\ kN}$$

Sliding limit check presented on equation (2.50);

$$\frac{|P| \cdot \tan\varphi}{H'} \geq 1.00$$

$$\frac{1773{,}9 \cdot \tan 33}{1499{,}50} = 0{,}77 < 1{,}00$$

2000 kN weight for towhead is not sufficient to prevent sliding, for further analysis of minimum weight, an excel spreadsheet is prepared by using the same equations.

Table 8-1: 2000 kN weight sliding check

Input data	Minimum weight	-2.000,00	(kN)
	friction angle	38	(˚)
	Reduction Factor	0,87	(-)
	Reduced sliding friction angle	33	(˚)
	B	6,00	(m)
	L	20,00	(m)
	Load Factor	1,00	(-)
	Material Factor	1,00	(-)
Trawl Load	F_x	0,00	(kN)
	F_y	226,08	(kN)
	F_z	621,14	(kN)
Loads at Geometric Center	F_x	0,00	(kN)
	F_y	-1.773,92	(kN)
	F_z	621,14	(kN)
	x (distance to GC)	10,00	(m)
	y (distance to GC)	3,50	(m)
	z (distance to GC)	3,00	(m)
	M_x	2.852,20	(kN.m)
	M_y	6.211,37	(kN.m)

	M_z	-2.260,75	(kN.m)
Effective Area	e_x	1,27	(m)
	e_z	1,61	(m)
	L_{eff}	17,45	(m)
	B_{eff}	2,78	(m)
	M_y	5.419,77	(kN.m)
	H'	1.499,56	(kN)
	Tan(phi-r)*lFyl	1.154,64	(kN)
	Sliding FoS	**0,77**	(-)

For the next step, towhead weight increased to 2540 kN and the minimum weight that can resist sliding of towhead is 2540 kN with the sliding factor of safety 1.00, as shown in Table 8-2.

Table 8-2: 2540 kN. weight sliding check

Input data	Minimum weight	-2.540,00	(kN)
	Friction angle	38	(˚)
	Reduction factor	0,87	(-)
	Reduced sliding friction angle	33	(˚)
	B	6,00	(m)
	L	20,00	(m)
	Load factor	1,00	(-)
	Material factor	1,00	(-)
Trawl Load	F_x	0,00	(kN)
	F_y	226,08	(kN)
	F_z	621,14	(kN)
Loads at Geometric Center	F_x	0,00	(kN)
	F_y	-2.313,92	(kN)
	F_z	621,14	(kN)
	x (distance to GC)	10,00	(m)
	y (distance to GC)	3,50	(m)
	z (distance to GC)	3,00	(m)
	M_x	2.852,20	(kN.m)
	M_y	6.211,37	(kN.m)
	M_z	-2.260,75	(kN.m)
Effective Area	e_x	0,98	(m)
	e_z	1,23	(m)
	L_{eff}	18,05	(m)
	B_{eff}	3,53	(m)
	M_y	5.604,50	(kN.m)
	H'	1.499,56	(kN)
	Tan(phi-r)*lFyl	1.506,13	(kN)
	Sliding FoS	1,00	(-)

8.1.2 Towhead foundation stability envelope

As explained earlier, to evaluate the towhead foundation ultimate capacity in presence of eccentric loading, it is recommended by DNV to construct a stability envelope, thus another excel spreadsheet is created for ultimate bearing capacity calculation, and the effective width and length of the foundation are considered in all steps,

Towhead ultimate bearing capacity is calculated using various H/V ratios, and the ultimate bearing capacity formula is rewritten using Brinch Hansen's approach, Equation (2.9),

$$q_u = \frac{1}{2}\gamma' b_{eff} N_\gamma S_\gamma d_\gamma i_\gamma + (P_0')N_q S_q d_q i_q$$

For the case of this study, towhead on sand without any surcharge, q_u can be written as follows;

$$q_u = \frac{1}{2}\gamma' b_{eff} N_\gamma S_\gamma d_\gamma i_\gamma$$

$$N_q = \exp(\pi \cdot \tan\varphi) \cdot \tan^2\left(\frac{\pi}{4} + \frac{\varphi}{2}\right) = \exp(\pi \cdot \tan 38) \cdot \tan^2\left(\frac{\pi}{4} + \frac{38}{2}\right) = 48{,}93$$

Bearing capacity factor N_γ is calculated following the recommendations of Caquot and Kerisel 1953 [1],

$$N_\gamma = 2\left(N_q + 1\right) \cdot \tan(\varphi) = 2 \cdot (48{,}93 + 1) \cdot \tan 38 = 77{,}9$$

Load inclination and shape factors are calculated according to [1],

$$S_\gamma = 1 - 0.4 \cdot \frac{i_\gamma \cdot b_{eff}}{l_{eff}}$$

$$i_\gamma = \left(1 - \frac{0.7 \cdot H}{V + A_{eff} \cdot c \cdot \cot\varphi}\right)^5$$

$$d_\gamma = 1.00$$

Table 8-3: Input data

Dead weight	-2540,00	(kN)
Vertical load	226,08	(kN)
Resultant horizontal force	1499,56	(kN)
Friction angle	38	(˚)
Reduction factor soil-steel	0,87	(-)
Reduced sliding friction angle	33	(˚)
B_{eff}	3,53	(m)
L_{eff}	18,05	(m)
A_{eff}	63,79	(m^2)
Unit weight	9,5	(kN/m^3)
N_q	48,9	(-)
N_γ	77,9	(-)

Load inclination and shape factors were calculated with different H/V ratios to define the bearing capacity. Tabulated results are presented in Table 8-4.

Table 8-4: Bearing capacity calculation

H/V (-)	i_γ (-)	S_γ (-)	q_u (kPa)	V (kN)	H (kN)
1,4	0,00	1,00	0,00	0,00	0,00
1,35	0,00	1,00	0,00	0,04	0,06
1,3	0,00	1,00	0,01	0,49	0,64
1,25	0,00	1,00	0,04	2,55	3,18
1,2	0,00	1,00	0,14	8,75	10,50
1,15	0,00	1,00	0,37	23,52	27,05
1,1	0,00	1,00	0,84	53,69	59,06
1,05	0,00	1,00	1,71	109,01	114,46
1	0,00	1,00	3,18	202,63	202,63
0,9	0,01	1,00	9,06	577,80	520,02
0,8	0,02	1,00	21,51	1.372,19	1.097,76
0,7	0,03	1,00	44,96	2.867,74	2.007,42
0,65	0,05	1,00	62,64	3.995,42	2.597,03
0,64	0,05	1,00	66,75	4.257,57	2.724,84
0,63	0,05	0,99	71,02	4.530,52	2.854,22
0,6	0,07	0,99	85,38	5.446,15	3.267,69
0,59	0,07	0,99	90,63	5.780,89	3.410,72
0,58	0,07	0,99	96,02	6.124,64	3.552,29
0,54	0,09	0,99	120,66	7.696,86	4.156,30
0,5	0,12	0,99	149,97	9.566,04	4.783,02
0,45	0,15	0,98	194,27	12.392,14	5.576,46
0,4	0,19	0,98	248,21	15.832,93	6.333,17
0,29	0,32	0,97	409,54	26.123,70	7.575,87
0,28	0,34	0,97	426,25	27.189,72	7.613,12
0,25	0,38	0,97	483,59	30.847,21	7.711,80
0,22	0,43	0,96	546,76	34.876,65	7.672,86
0,21	0,45	0,96	568,89	36.288,01	7.620,48
0,2	0,47	0,96	591,68	37.741,77	7.548,35
0,19	0,49	0,96	615,14	39.238,62	7.455,34
0,18	0,51	0,96	639,29	40.779,25	7.340,27

0,17	0,53	0,96	664,14	42.364,34	7.201,94
0,16	0,55	0,96	689,70	43.994,53	7.039,12
0,15	0,57	0,95	715,97	45.670,47	6.850,57
0,14	0,60	0,95	742,97	47.392,78	6.634,99
0,13	0,62	0,95	770,71	49.162,07	6.391,07
0,12	0,64	0,95	799,19	50.978,91	6.117,47
0,11	0,67	0,95	828,43	52.843,85	5.812,82
0,1	0,70	0,94	858,43	54.757,44	5.475,74
0,09	0,72	0,94	889,20	56.720,16	5.104,81
0,08	0,75	0,94	920,75	58.732,50	4.698,60
0,07	0,78	0,94	953,08	60.794,89	4.255,64
0,06	0,81	0,93	986,20	62.907,75	3.774,46
0,05	0,84	0,93	1020,12	65.071,43	3.253,57
0,04	0,87	0,93	1054,84	67.286,26	2.691,45
0,03	0,90	0,93	1090,37	69.552,54	2.086,58
0,02	0,93	0,92	1126,71	71.870,51	1.437,41
0,01	0,97	0,92	1164,21	74.262,41	742,62
0,001	1,00	0,92	1201,29	76.627,76	76,63
0,0001	1,00	0,92	1205,05	76.867,55	7,69
0,00001	1,00	0,92	1205,43	76.891,56	0,77
0,000001	1,00	0,92	1205,46	76.893,99	0,08
0,0000001	1,00	0,92	1205,47	76.894,21	0,01
0,00000001	1,00	0,92	1205,47	76.894,23	0,00

As discussed earlier in section 2.3.1, the foundation stability envelope is shown below, Reduced sliding friction angle of 33° is used to draw the line of sliding failure.

As it can be seen from Figure 8-2, the minimum weight of 2540 kN is safe against sliding and bearing failure of foundation and the resultant vertical and horizontal forces are 2313.92 kN and 1499.56 kN accordingly.

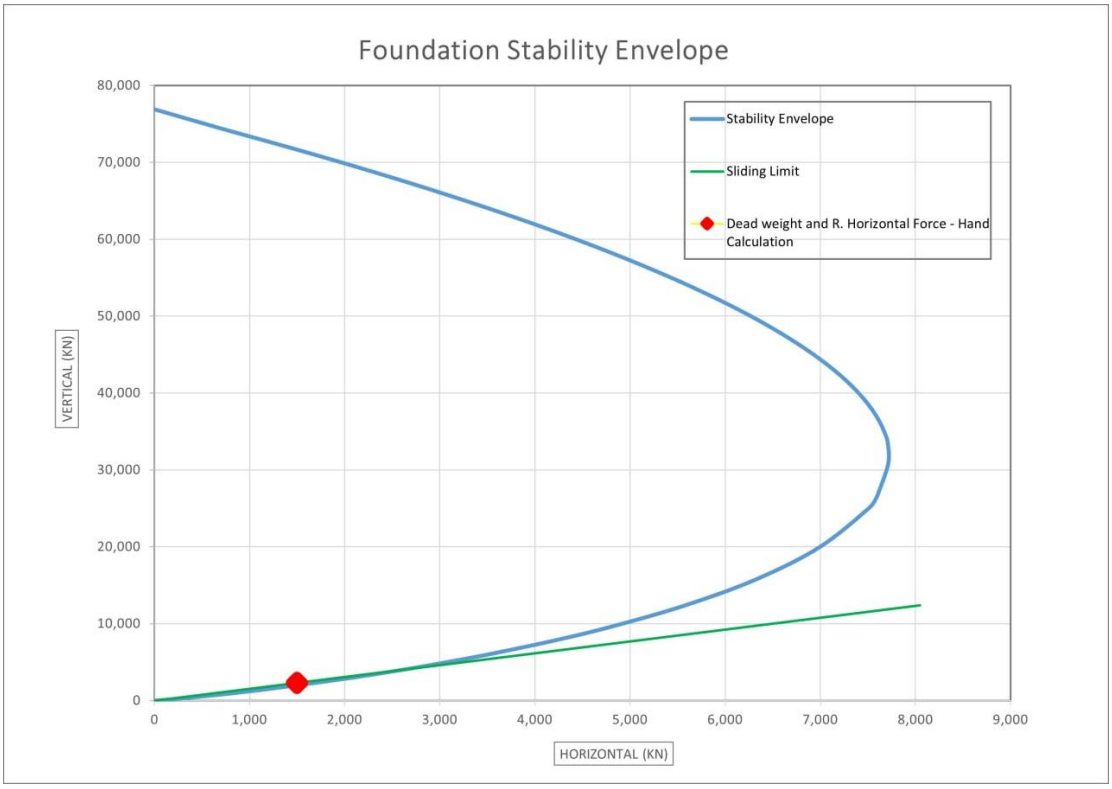

Figure 8-2: Foundation stability envelope